Material behavior and manufacturing solutions for biomedical applications: from computational optimization to 3D printing

Gianluca Alaimo

Supervisor: Prof. Ferdinando Auricchio

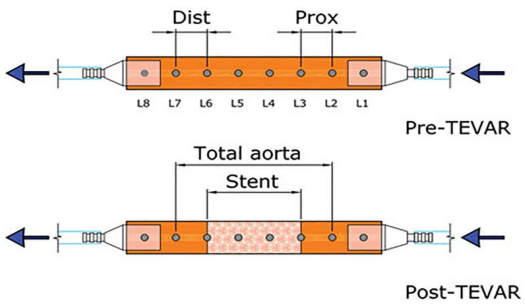

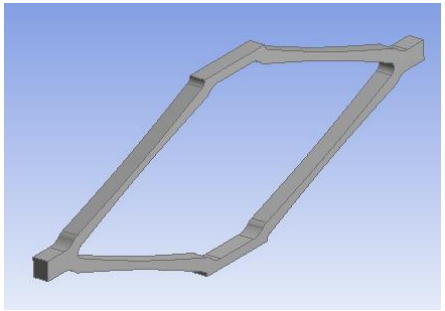

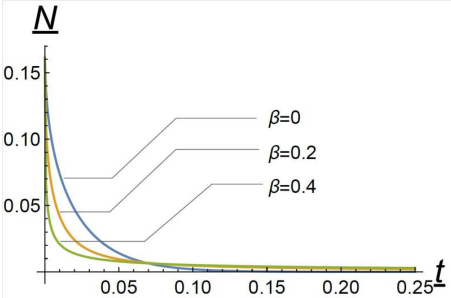

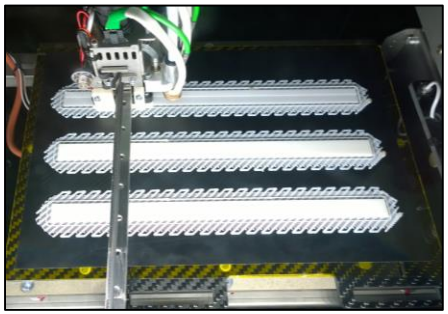

Outline

UNIVERSITÀ DI PAVIA

Medical devices

- Impact of TEVAR on longitudinal strain
- Multi-objective optimization of Nitinol stent design

Non-Fourierian Heat Conduction

- Anomalous heat conduction
- Thermo-mechanical coupling

3D Printing

- Influence of meso-structure and chemical composition on FDM 3D-printed parts

Outline

UNIVERSITÀ DI PAVIA

Medical devices

- Impact of TEVAR on longitudinal strain
- Multi-objective optimization of Nitinol stent design

Non-Fourierian Heat Conduction

- Anomalous heat conduction
- Thermo-mechanical coupling

3D Printing

- Influence of meso-structure and chemical composition on FDM 3D-printed parts

Objectives and methods

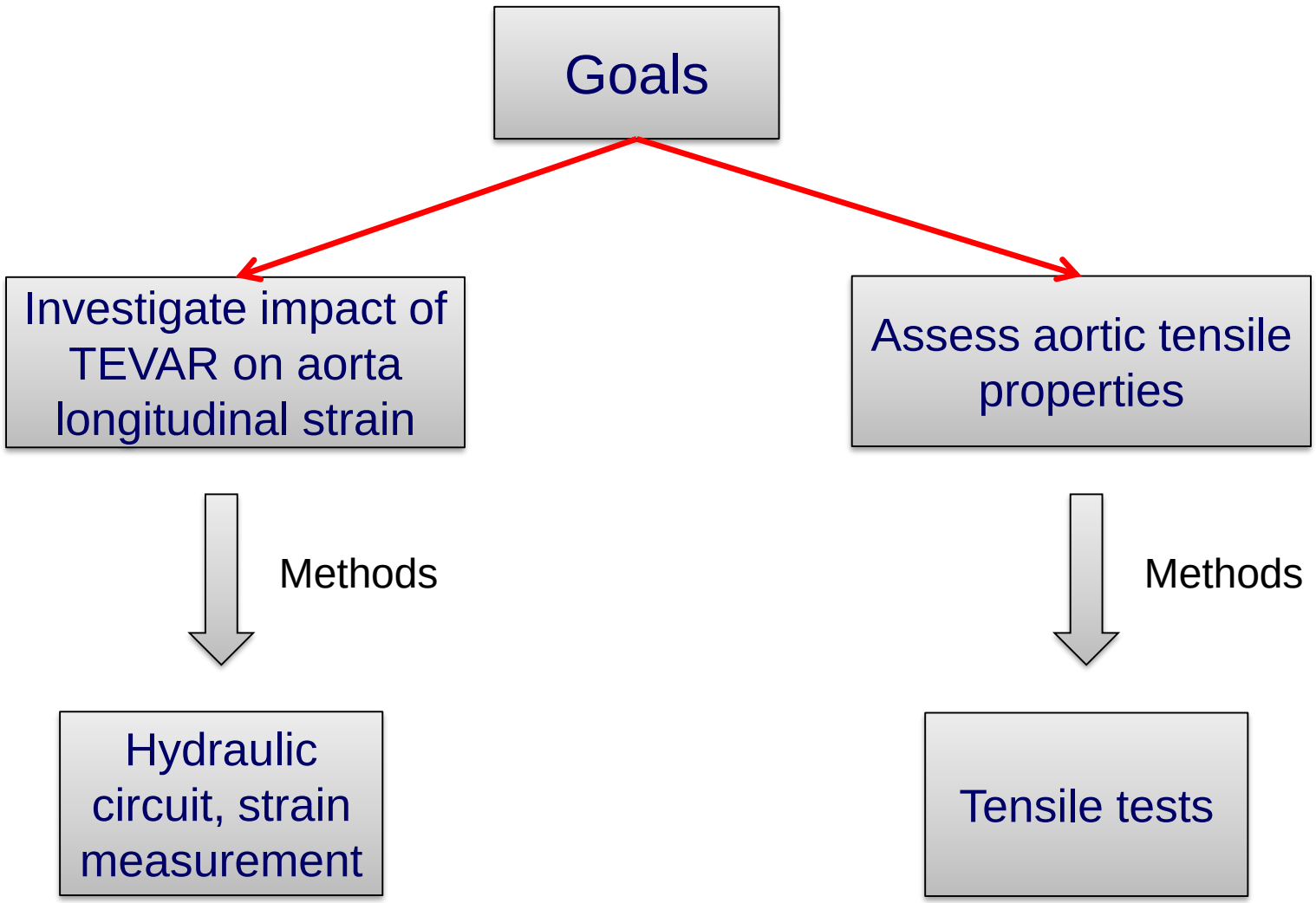

Strain measurement

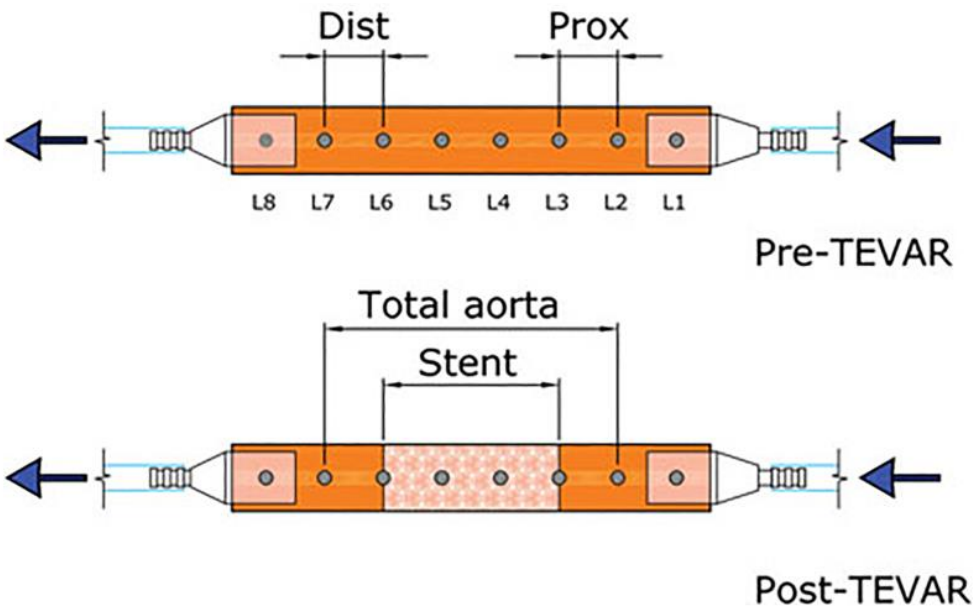

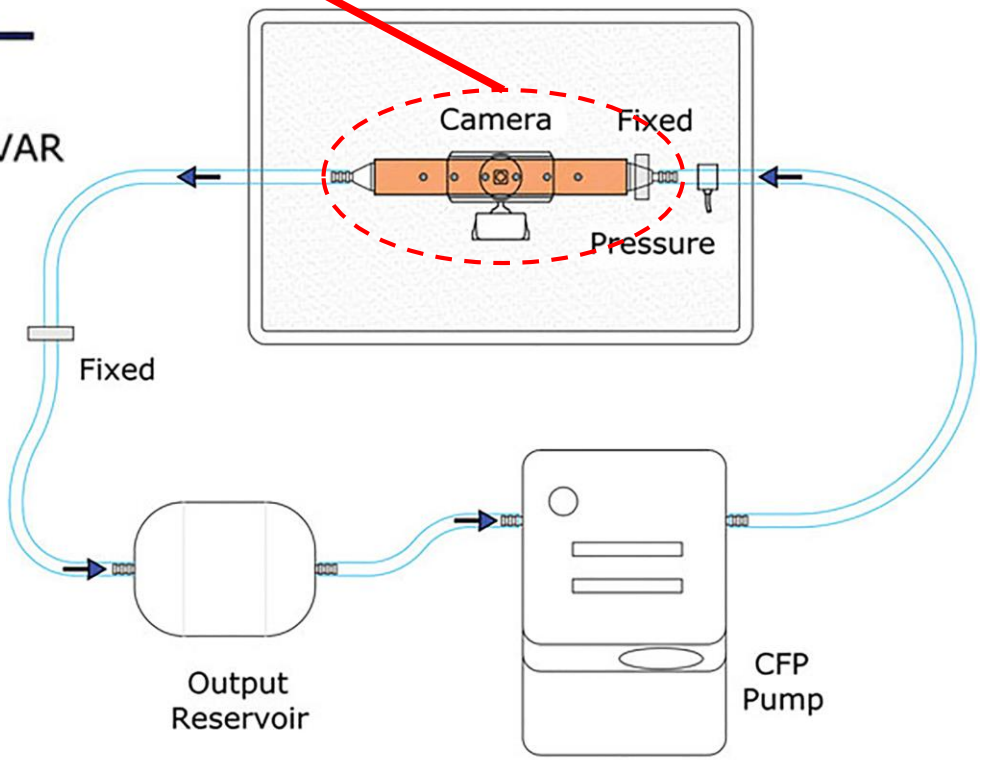

Results

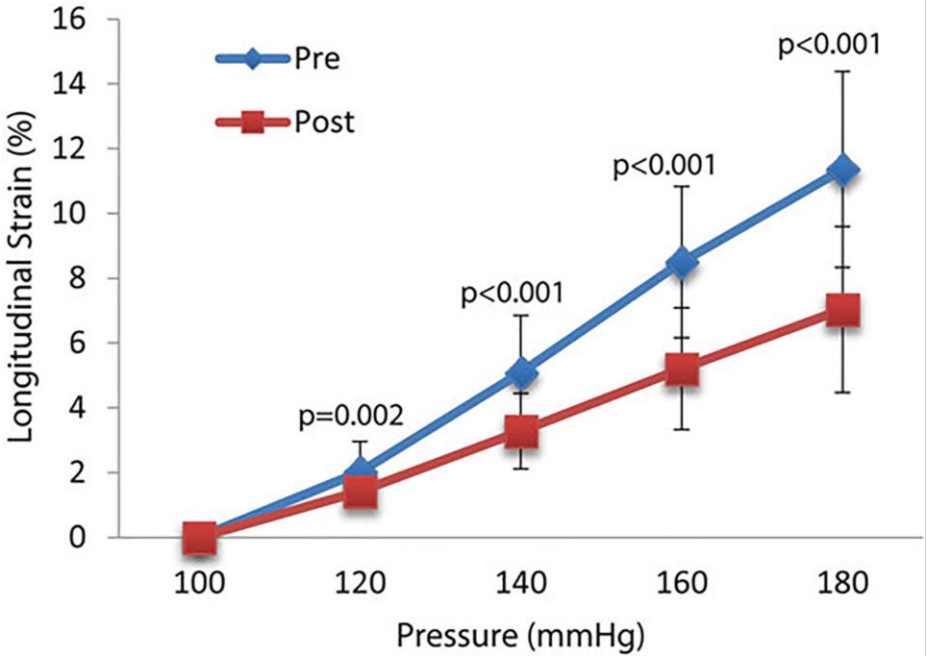

Total aorta

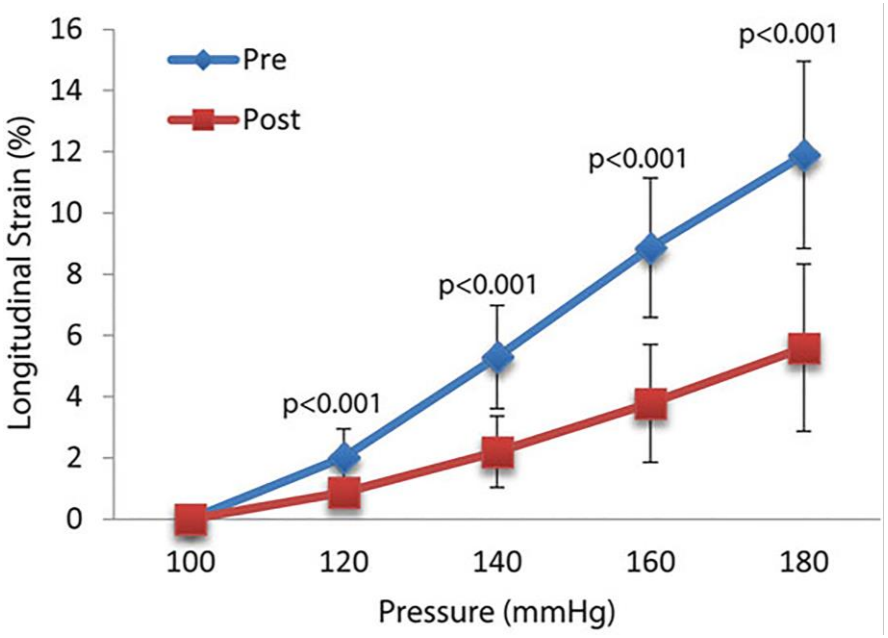

Stented segment

Results

Mean longitudinal strain at 180 mmHg

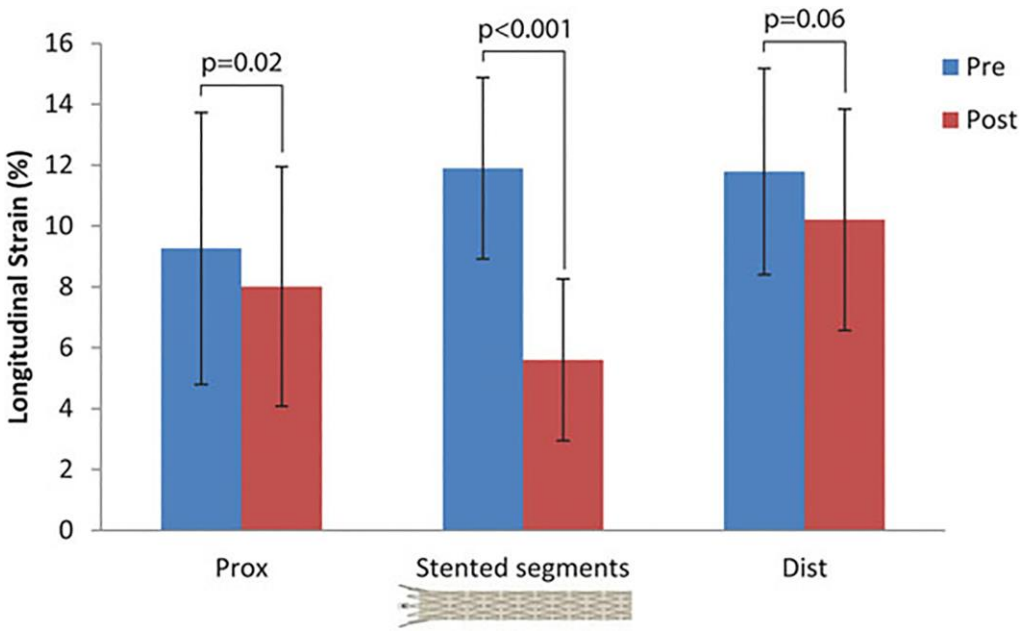

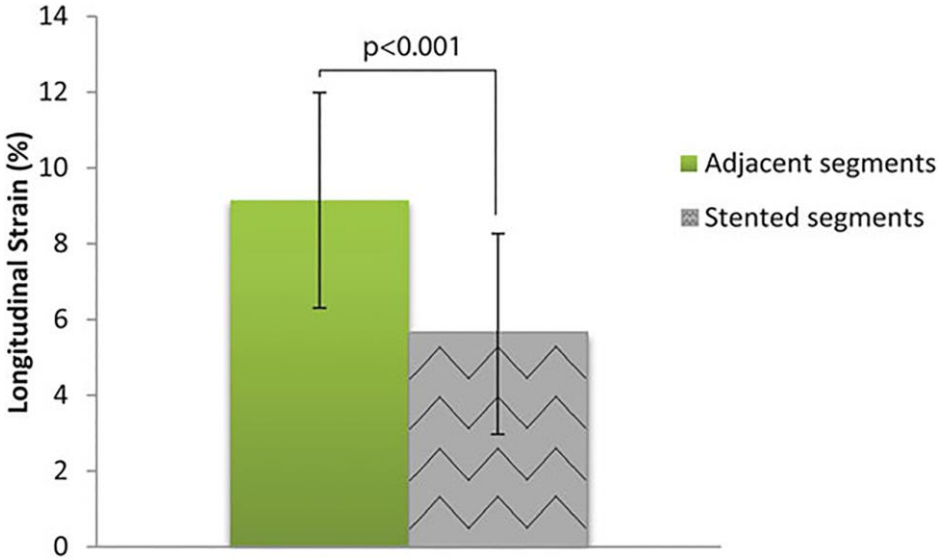

Results

A

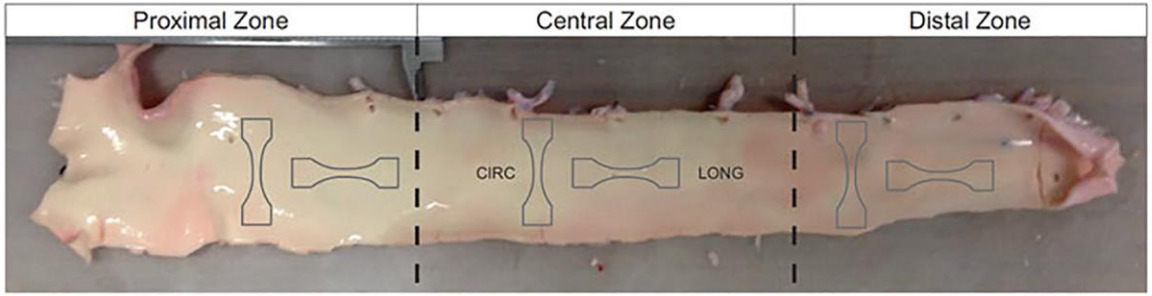

B

C

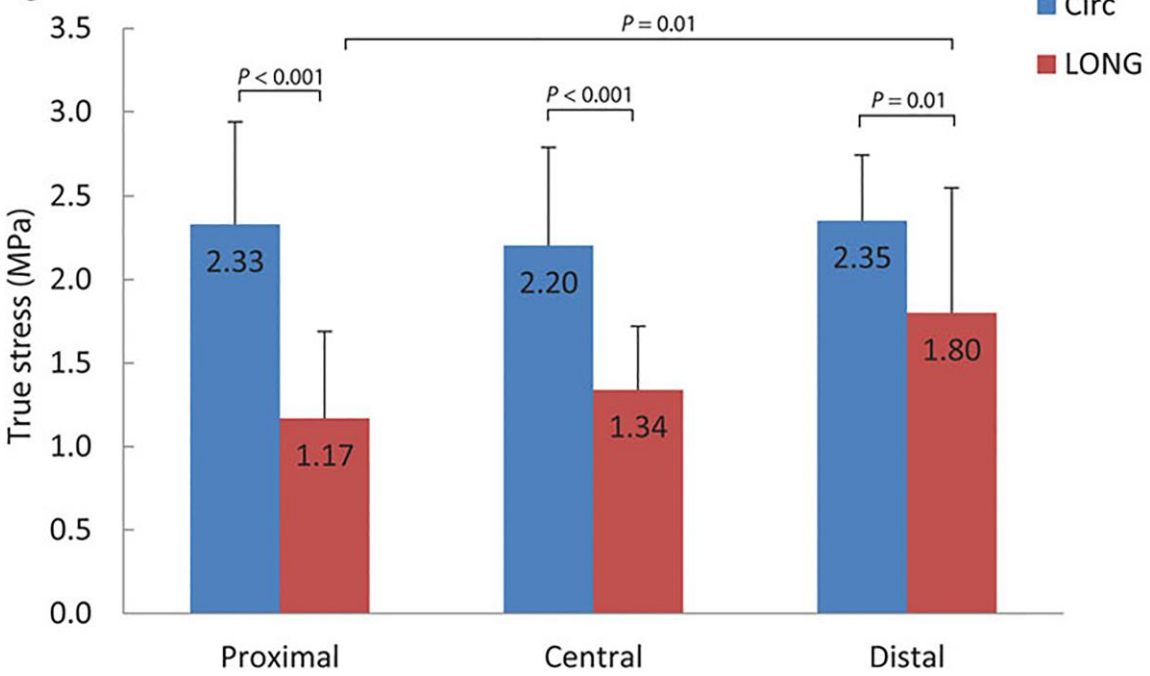

D

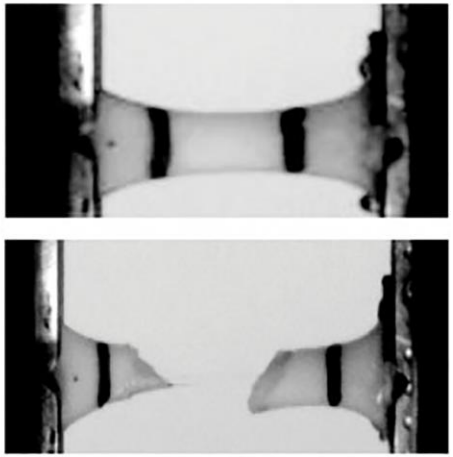

Conclusions

- TEVAR induced a longitudinal strain decrease from *11.9%* to *5.6%* in the stented segments
- TEVAR induced a longitudinal strain mismatch between stented (*5.6%*) and non-stented segments (*9.1%*)
- Tensile testing showed that peak stress was lower for longitudinal (*1.4MPa*) than for circumferential fragments (*2.3MPa*)
- Longitudinal fragments were more prone to rupture proximally than distally

Outline

UNIVERSITÀ DI PAVIA

Medical devices

- Impact of TEVAR on longitudinal strain
- Multi-objective optimization of Nitinol stent design

Non-Fourierian Heat Conduction

- Anomalous heat conduction
- Thermo-mechanical coupling

3D Printing

- Influence of meso-structure and chemical composition on FDM 3D-printed parts

Nitinol stent failure

Stent failures with a rate of 37% after 9 months

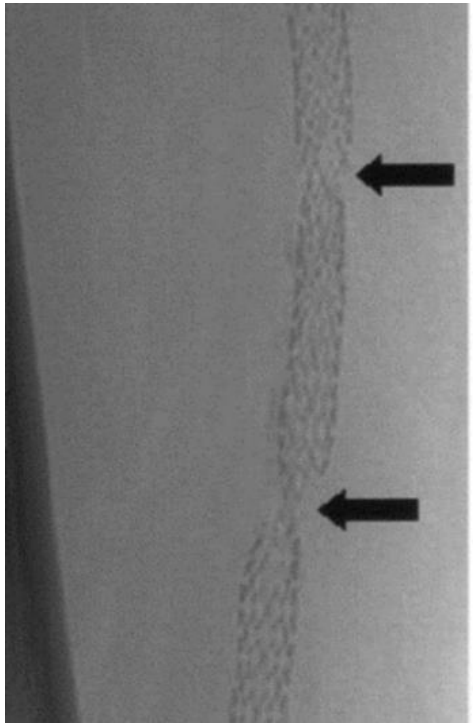

Restenosis and reduction of vessel diameter

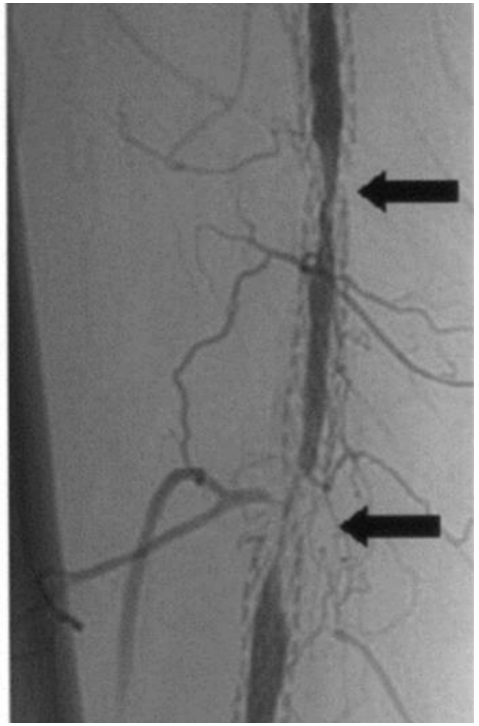

[Scheninert et al. 2005]

Fatigue failure

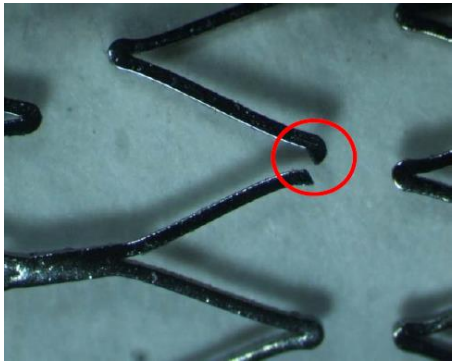

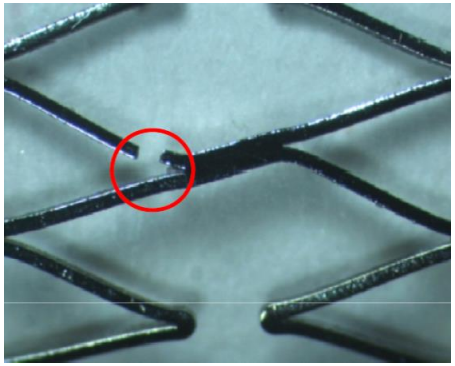

[Petrini et al. 2013]

Objectives and methods

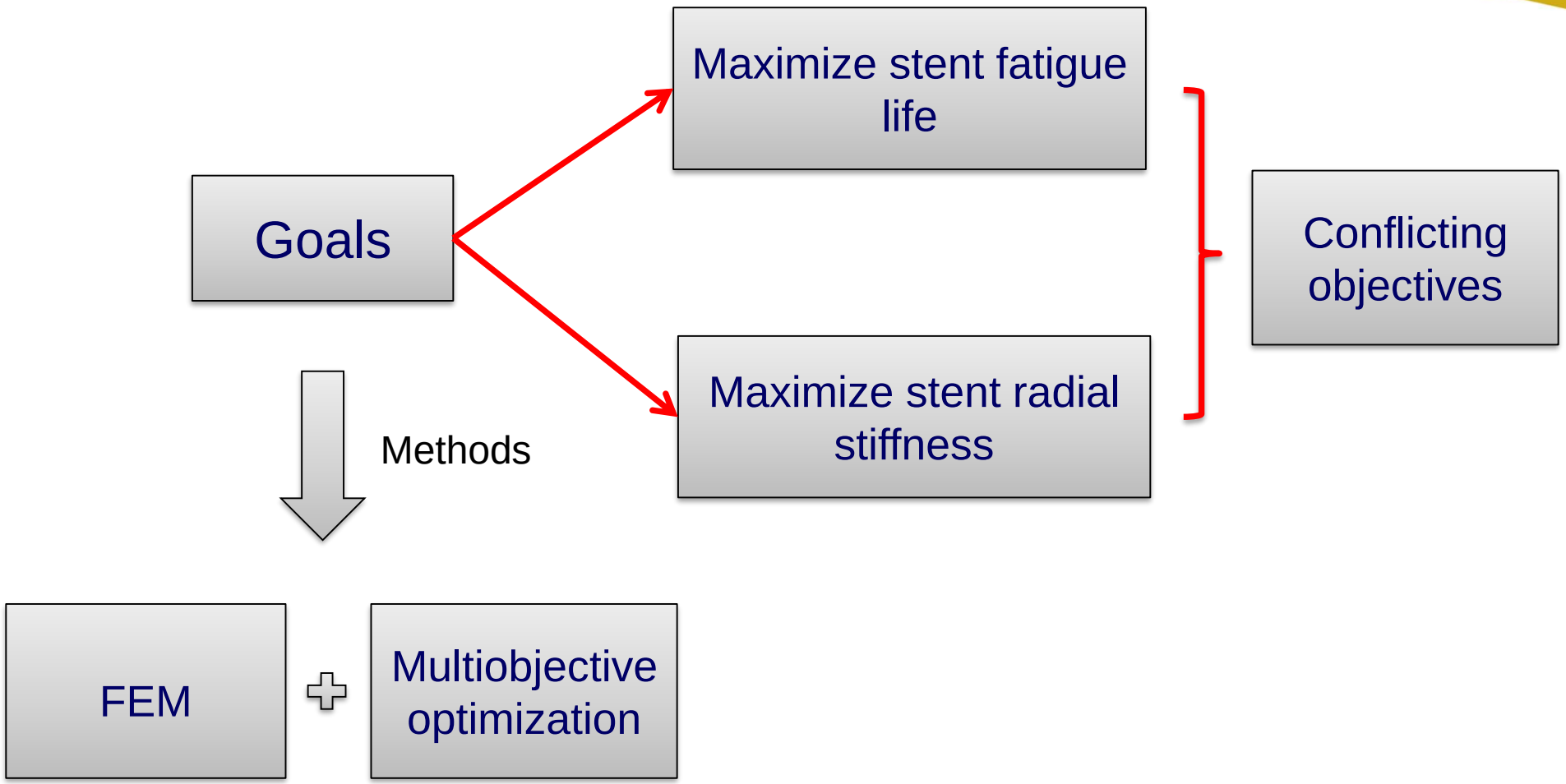

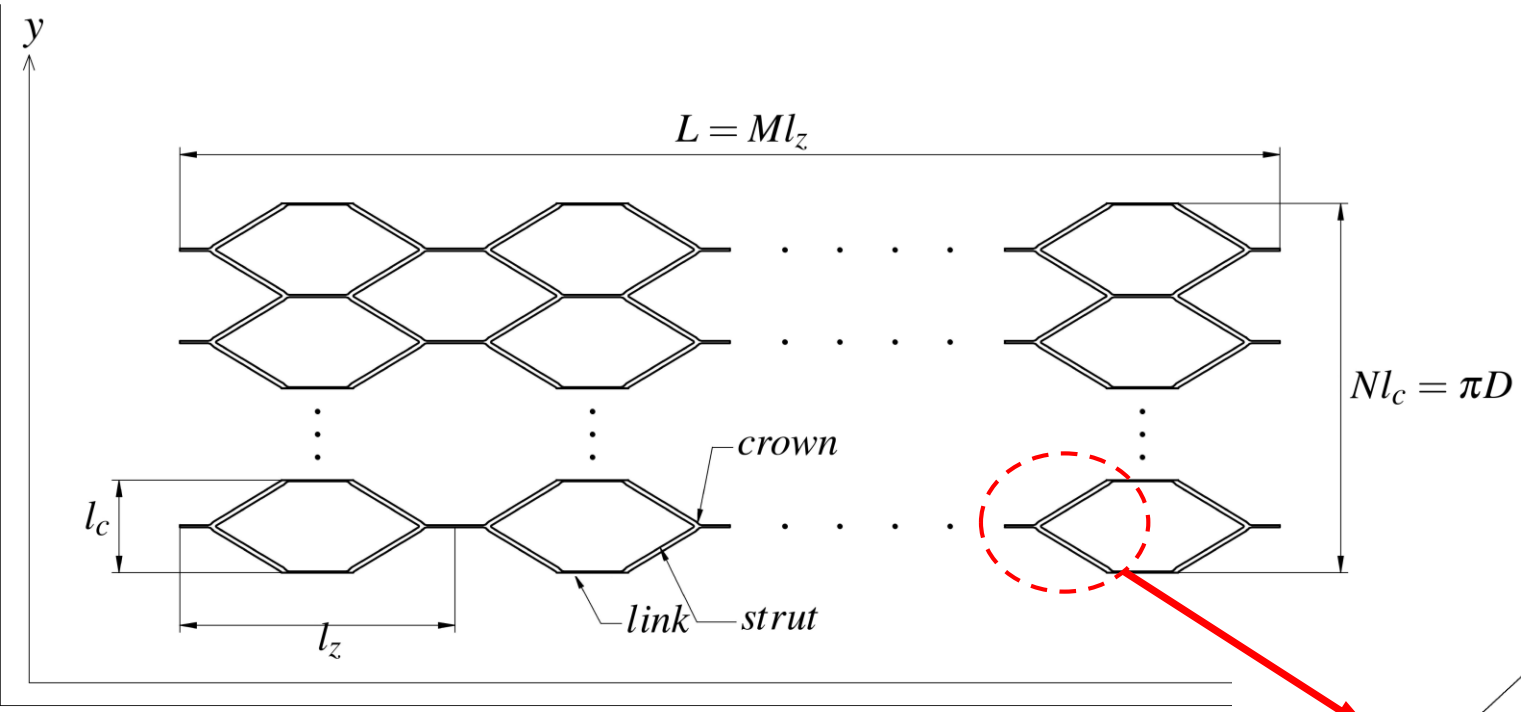

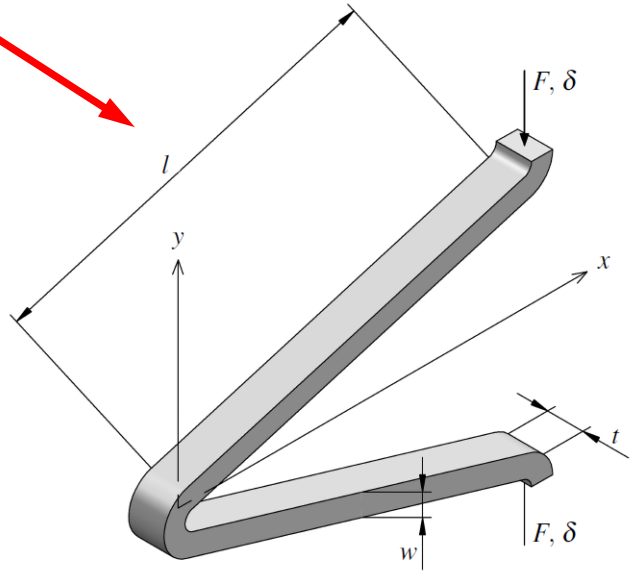

Optimization is performed on the stent cell

Optimization workflow

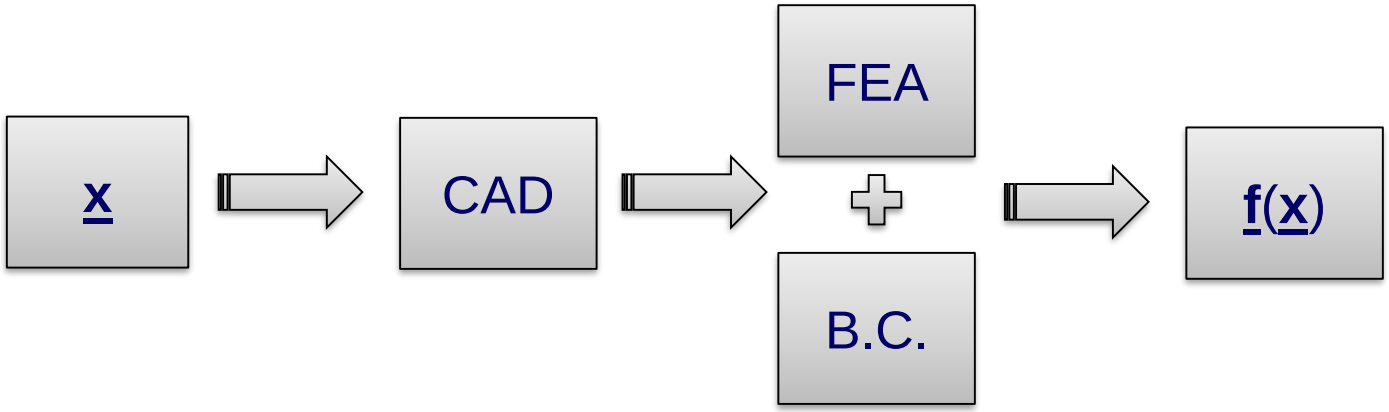

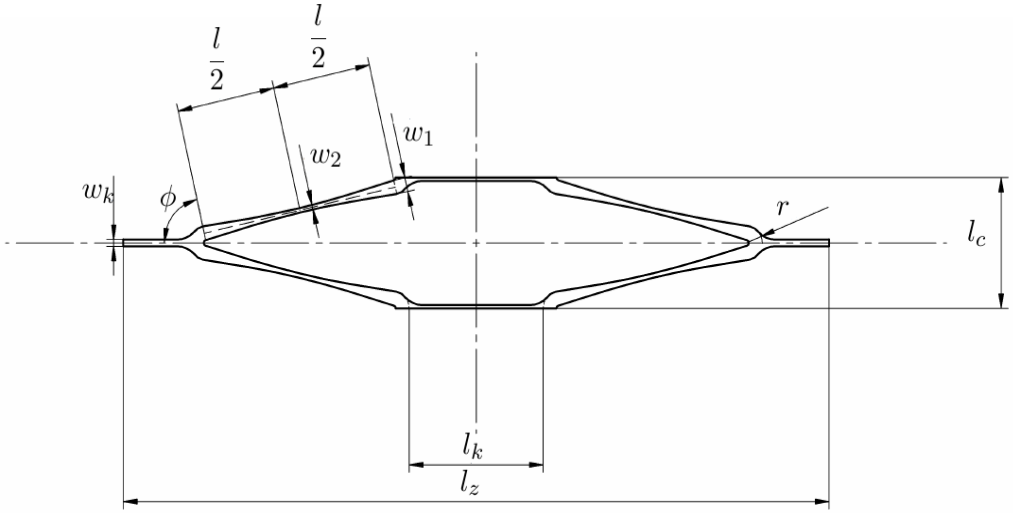

$$\underline{\mathbf{x}} = \left[\ w_1,\quad l,\quad a,\quad b,\quad c\ \right]^T \quad a = \frac{w_2}{w_1},\ b = \frac{r}{w_1},\ c = \frac{w_k}{w_1}$$

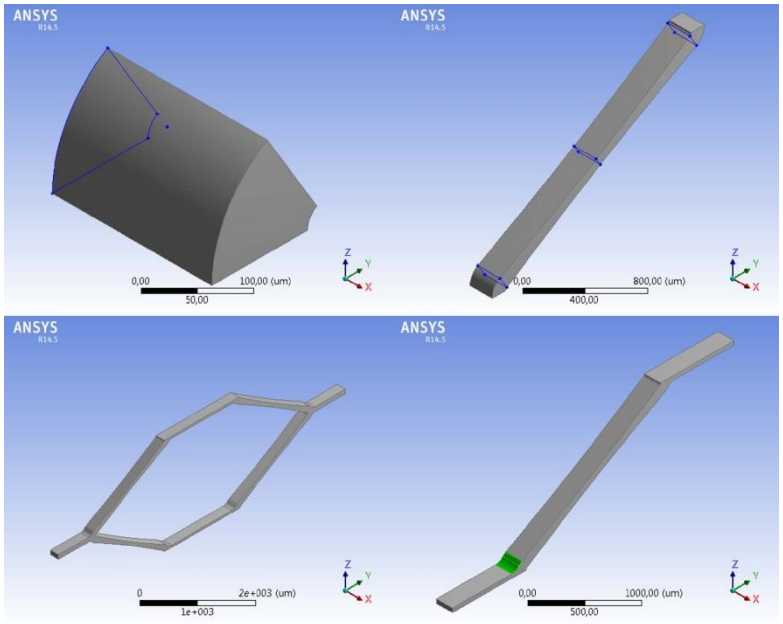

Optimization workflow

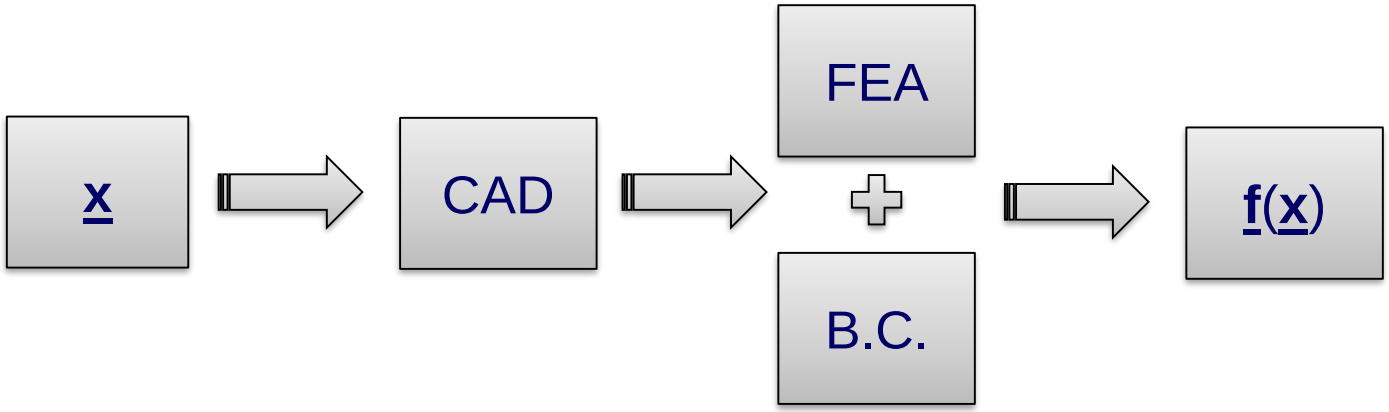

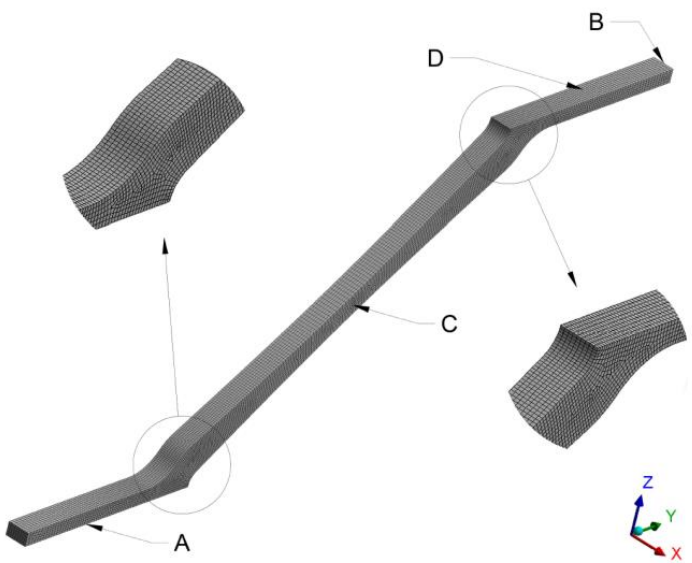

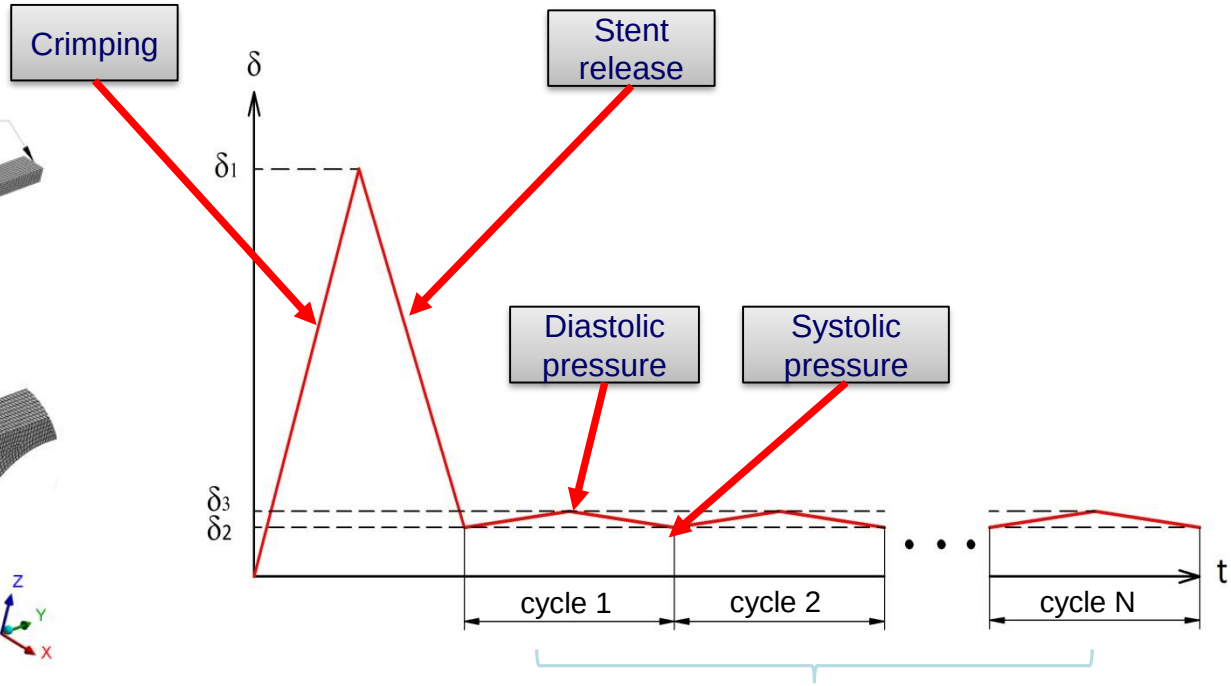

Fatigue Million Cycles

Optimization workflow

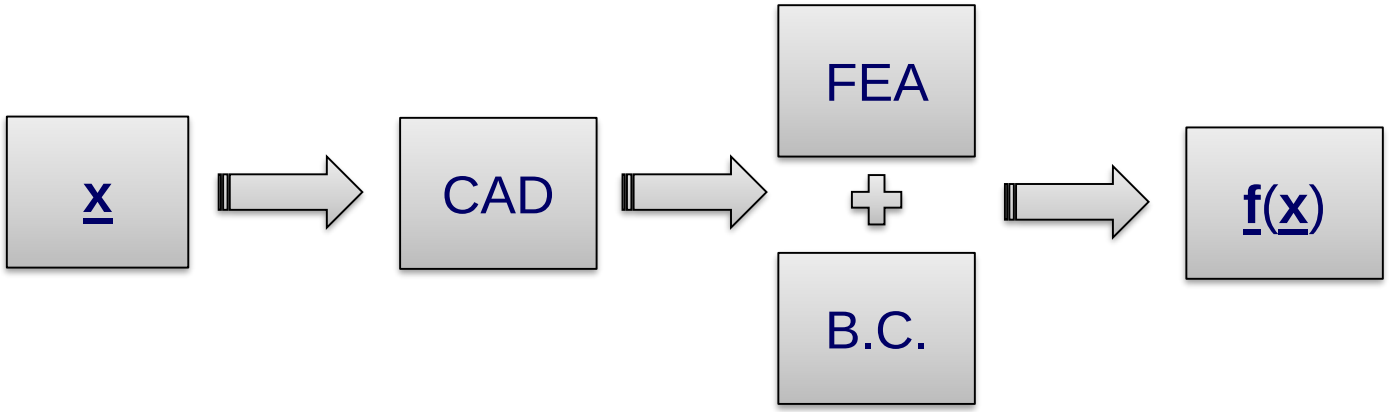

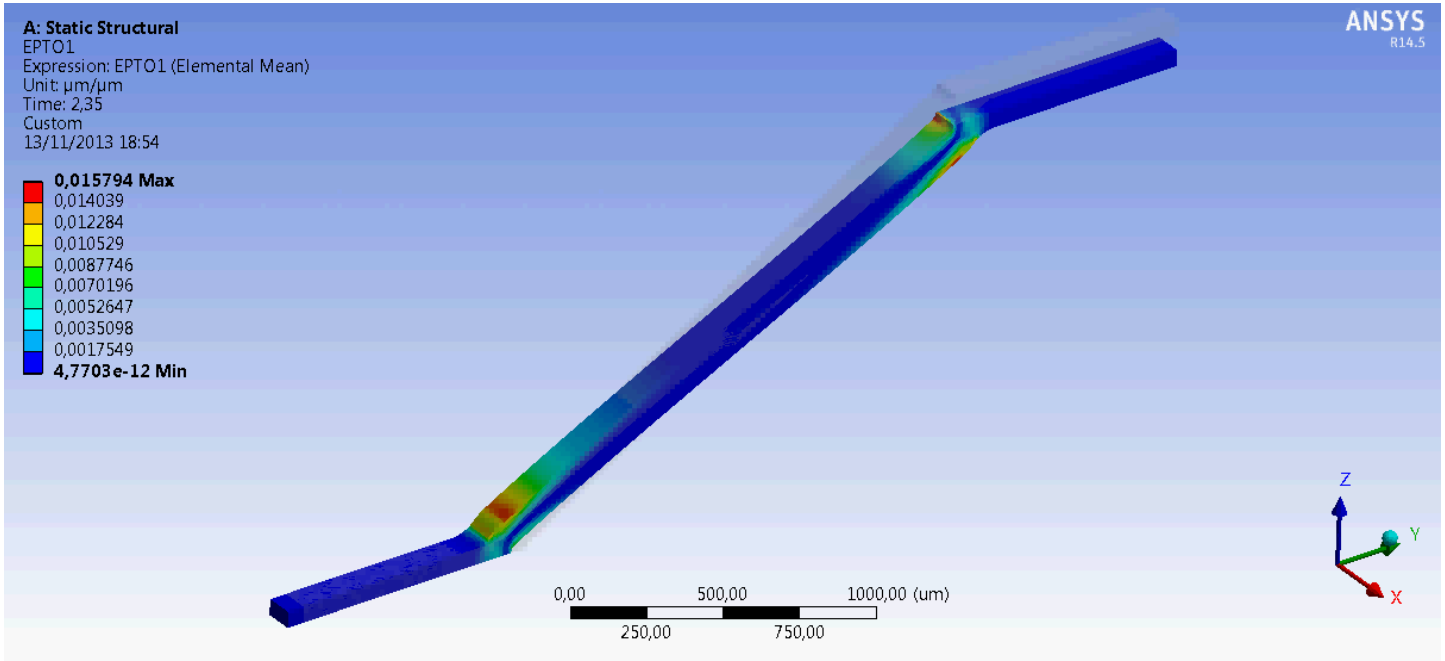

Optimization workflow

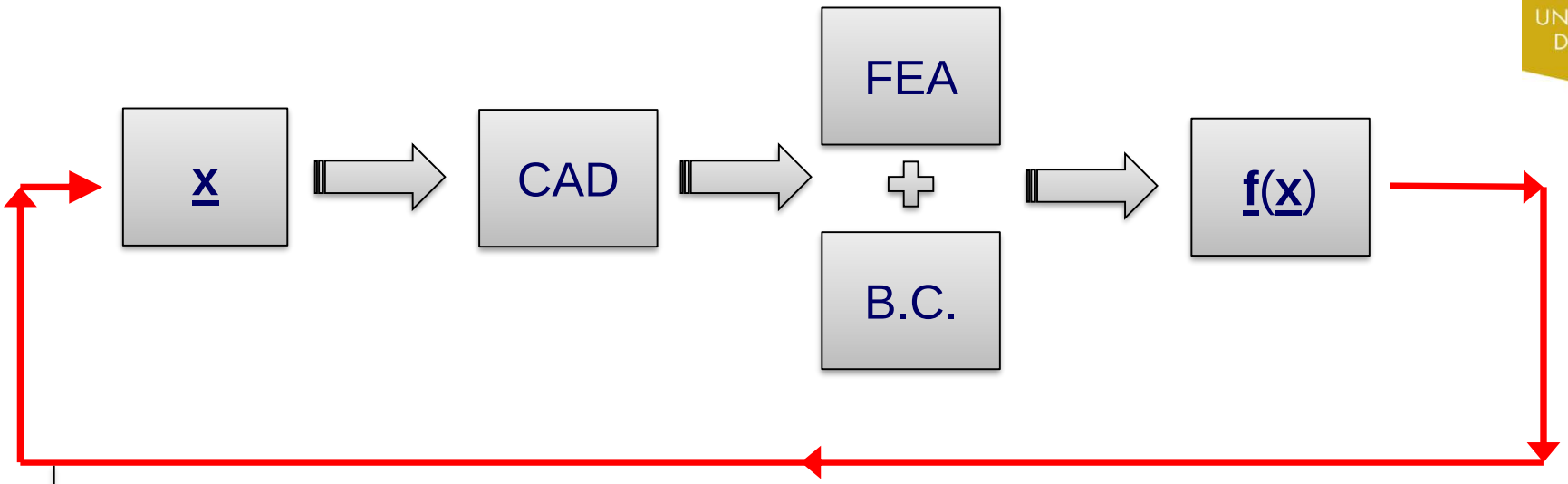

DOE

Response Surfaces

54 FE analises

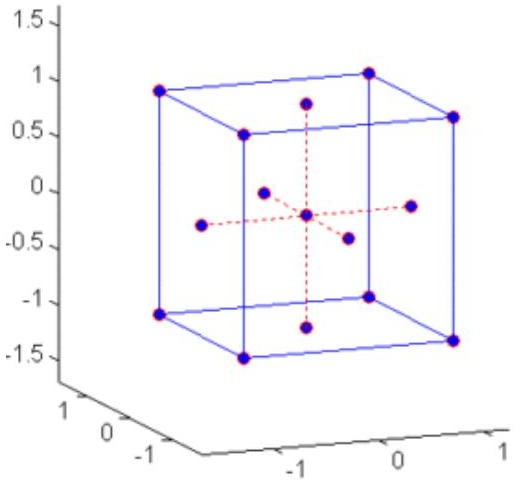

Optimization

Optimization workflow

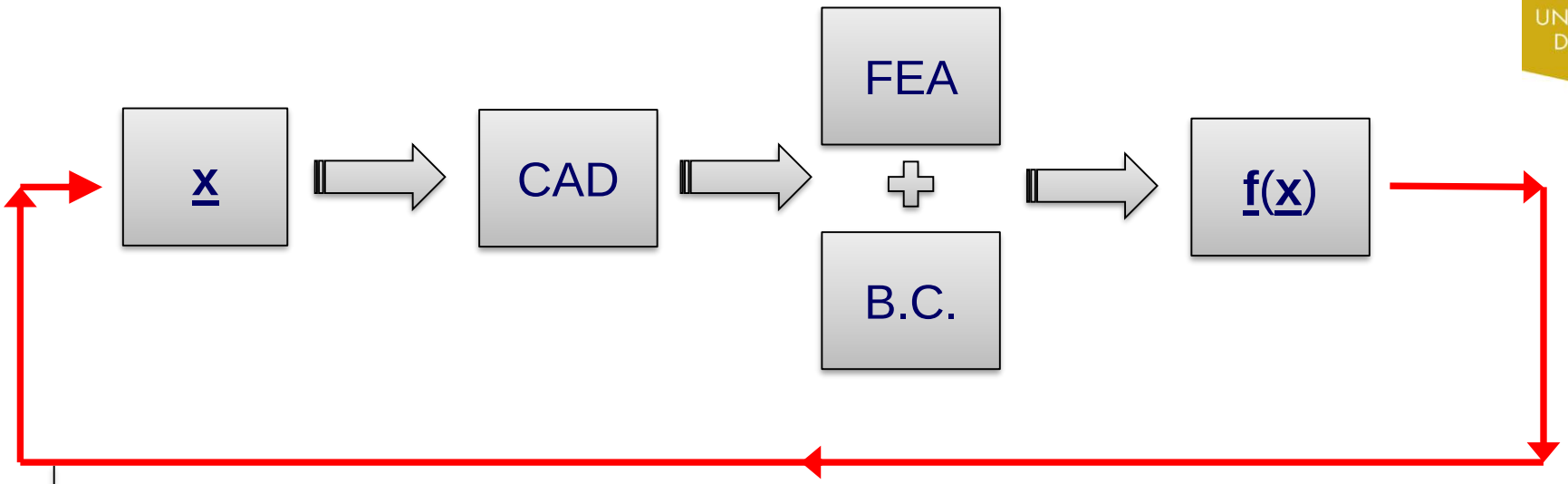

DOE

Response Surfaces

Kriging RS:
44 FE
analises

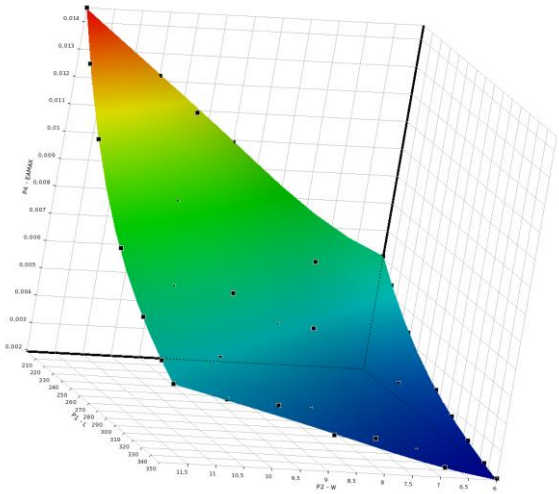

Optimization

Optimization workflow

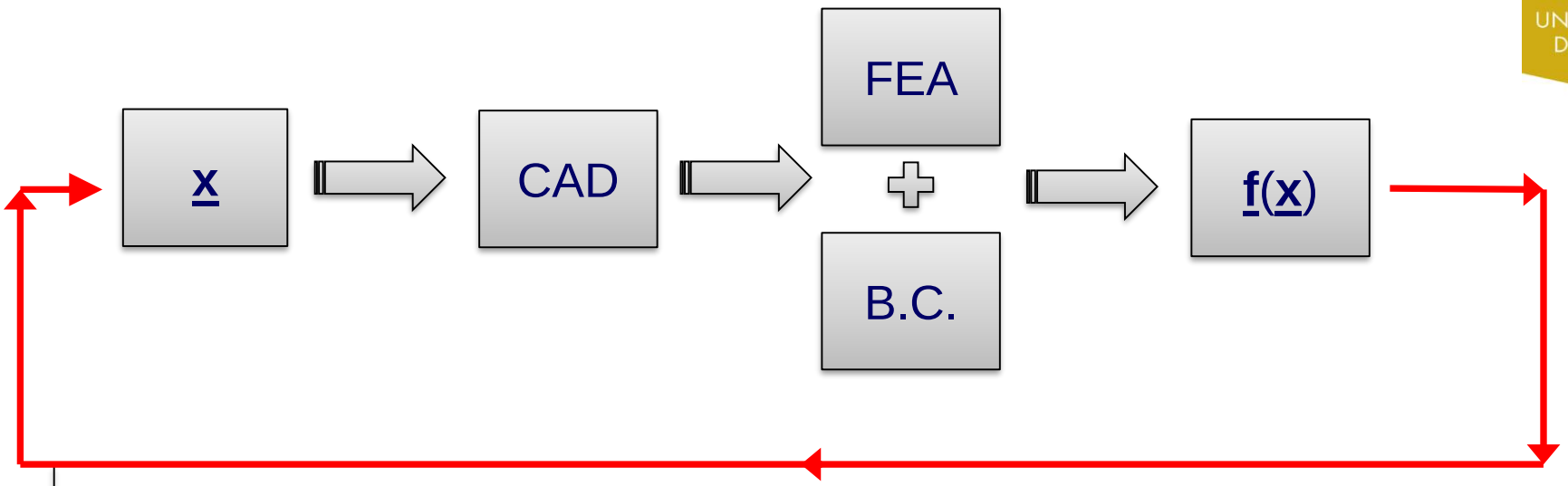

DOE

Response Surfaces

MOGA Genetic Algorithm

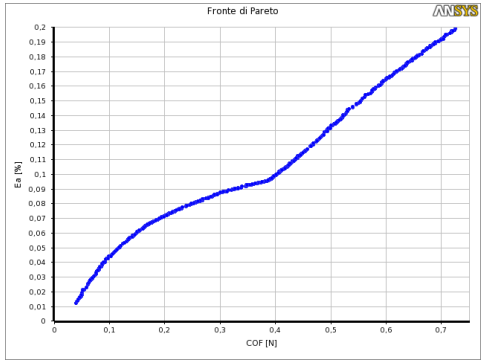

Optimization

Results

S_R =0,4/0,19=2,1

S_o =0,4/0,08=5

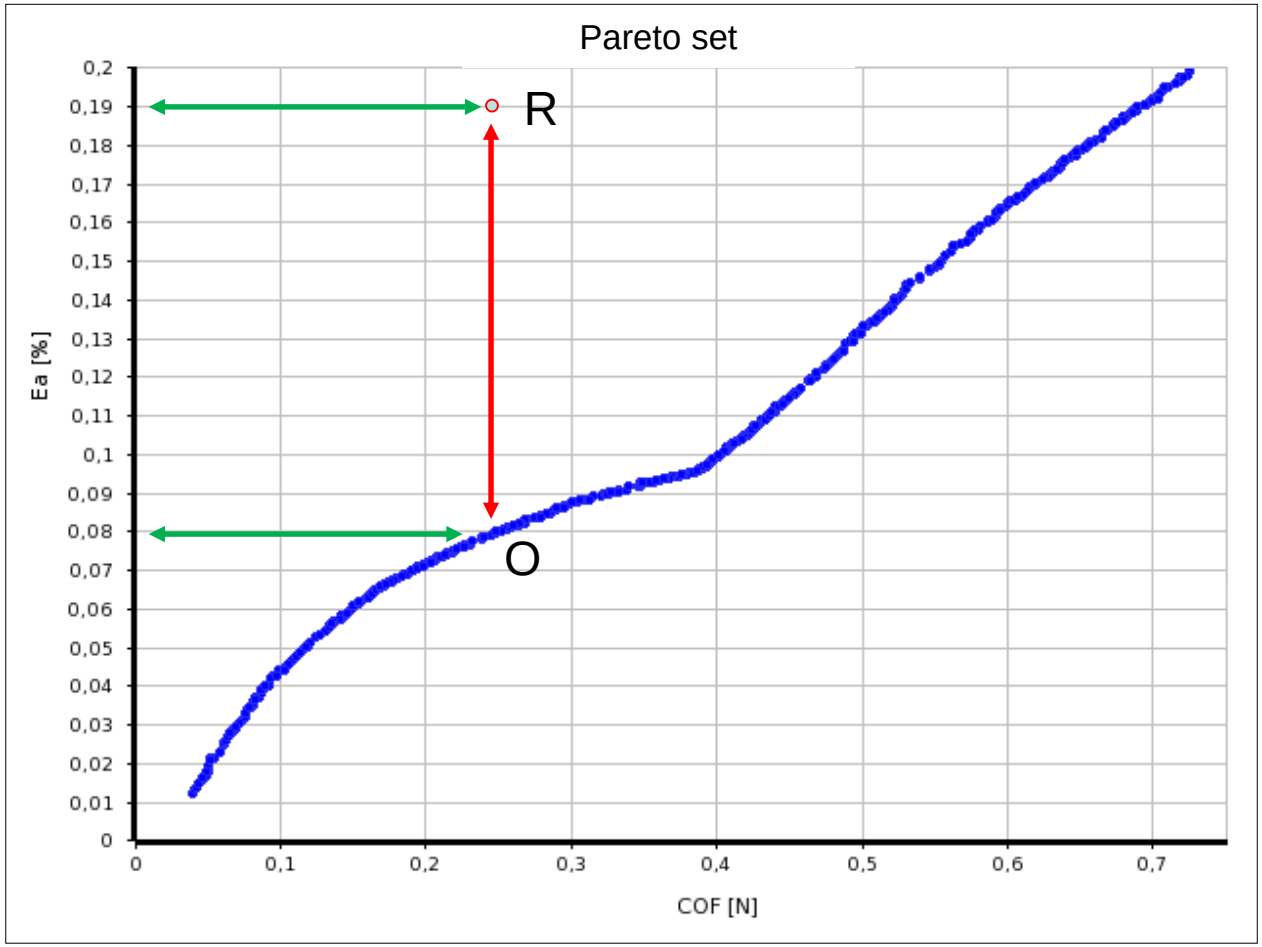

Results

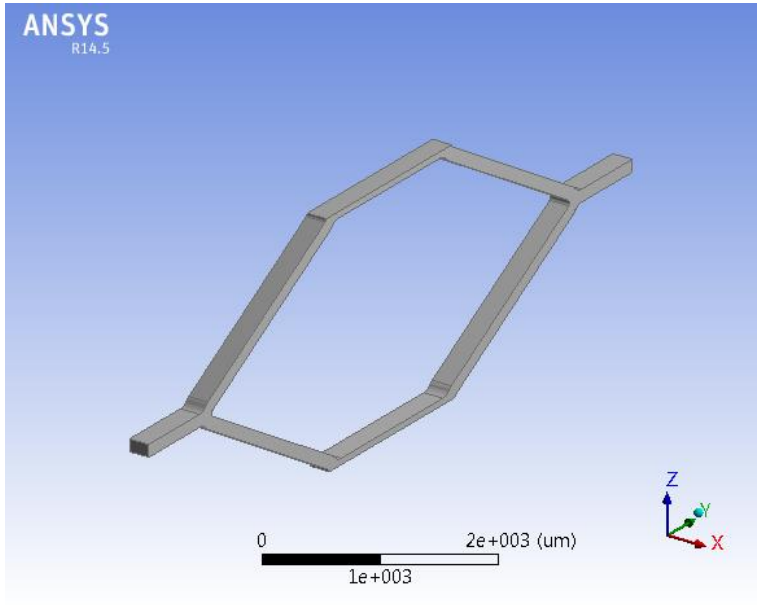

Shape optimization

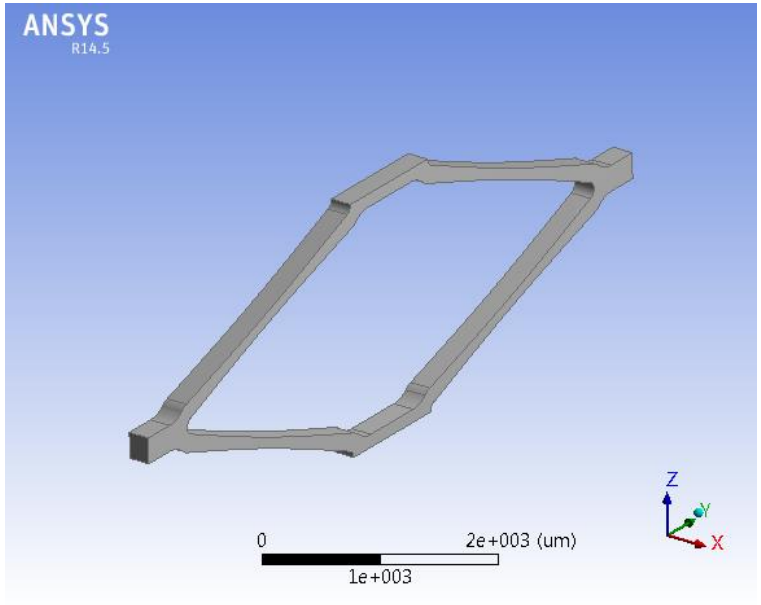

Reference design - S=2,1

Optimized design - S=5

Results

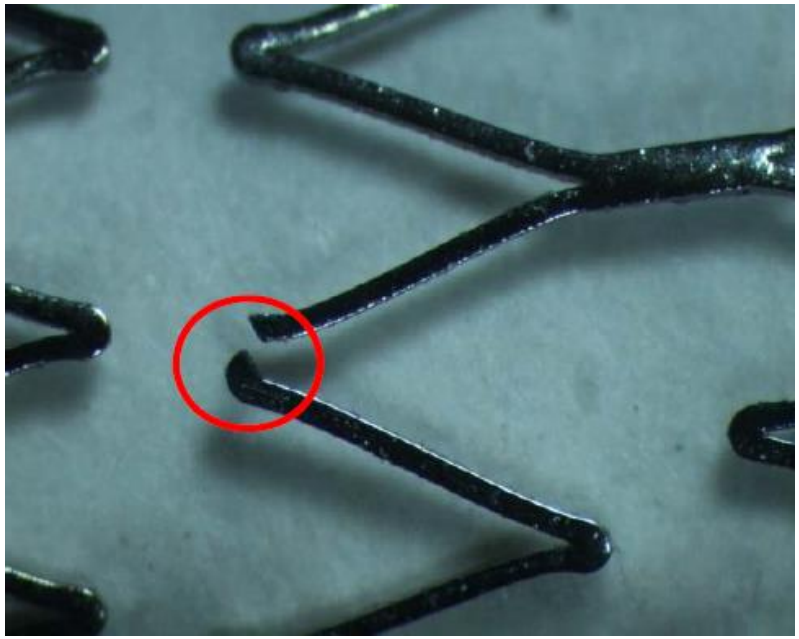

[Petrini et al. 2013]

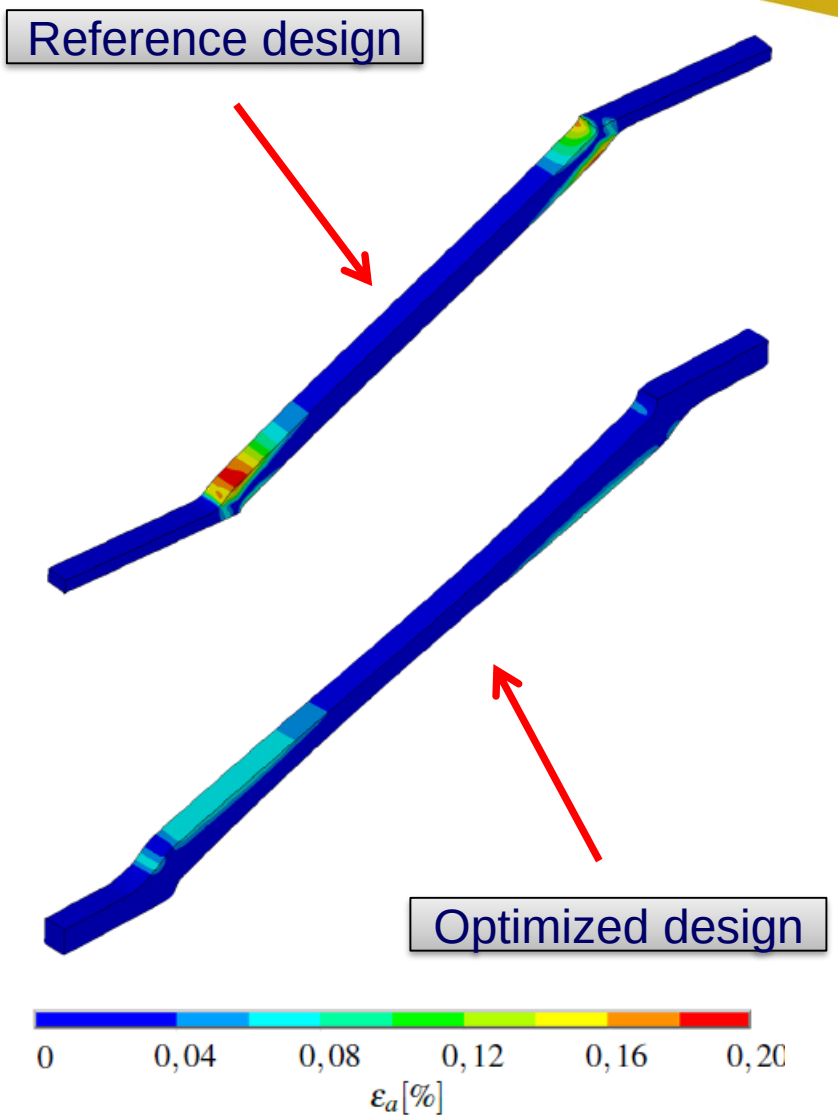

Conclusions

- The obtained Pareto set allows the designer to select the optimal solutions, according to the specific design requirements.

- Enhancement of stent fatigue life can be obtained combining tapered strut profile with the following changes in the cell design:
  - an increase of 25% of the strut length
  - an increase of 40% of the strut width at its extremities.

- Under such indications, it is possible to achieve a marked improvement of the fatigue safety factor, i.e., about *2.4* times, compared to the typical design (strut with constant section), without any loss of scaffolding capabilities

Outline

UNIVERSITÀ DI PAVIA

Medical devices

- Impact of TEVAR on longitudinal strain
- Multi-objective optimization of Nitinol stent design

Non-Fourierian Heat Conduction

- Anomalous heat conduction
- Thermo-mechanical coupling

3D Printing

- Influence of meso-structure and chemical composition on FDM 3D-printed parts

Anomalous heat transfer

Unpredicted (non-Fourierian) effects in heat transport

- Nano-tubes
- Resins
- Biological tissues
- Fiber composites
- Inert non homogeneus solids
- Combustion in solid reagents

References

[1] Antaki, P.J. , «Importance of non-Fourier heat conduction in solid-phase reactions", *Combustion and Flame*, 112, (1998)

[2] Atanackovic, T.M. et al. , "Time distributed-order diffusion-wave equation. I. Volterra-type equation», *Continuum Mech. Thermodyn.*, 24 (2012)

[3] Banerjee, A. et al. , «Temperature Distribution in Different Materials Due to Short Pulse Laser Irradiation», *Heat Transfer Engineering,* 26, (2005)

[4] Cattaneo, C. , «Sulla conduzione del calore», *Atti Seminario Mat. Fis.,* University Modena, 3, (1948)

[5] Chang, C.W. Et al. , «Breakdown of Fourier's Law in Nanotube Thermal Conductors", *Physical Review Letters*, 101, (2008)

[6] Davydov, E.V. et al. , «Non-diffusive heat transfer in muscle tissue. Preliminary results", *Russian Academy of Sciences*, (2008)

[7] Di Paola, M. et al., "Exact mechanical models of fractional hereditary materials», *J. Rheol.* 56, (2012)

[8] Ezzat, M.A. et al. , "Fractional Order Theory of Thermoelastic Diffusion", *Journal of Thermal Stresses,* 34, (2011)

[9] Gurtin, M.E. et al. , «A general theory of heat conduction with finite wave speeds», *Archive for Rational Mechanics and Analysis,* 31, (1968)

[10] Povstenko, Y. Z. , «Theory of thermoelasticity based on the space-time-fractional heat conduction equation», *Physica Scripta,* 136, (2009)

[11] Xu, F. et al. , «Non-Fourier analysis of skin biothermomechanics", *International Journal of Heat and Mass Transfer,* 51 (2008)

Transport equation/heat conduction equation

UNIVERSITÀ DI PAVIA

Fourier ⇒ $$\mathbf{q} = -\lambda \frac{\partial^0}{\partial t^0} \nabla T$$

Fractional Fourier equation ⇒ $$\mathbf{q} = -\lambda_\beta \left({}_C\mathrm{D}_0^\beta f \right)(t) \qquad 0 \le \beta < 1$$

where $\left({}_C\mathrm{D}_0^\beta f \right)(t) = \frac{1}{\Gamma(1-\beta)} \int_0^t \frac{f'(\tau)}{(t-\tau)^\beta} d\tau.$ is the Caputo fractional derivative

$\Gamma(z) = \int_0^\infty e^{-x} x^{z-1} dx.$ is the Euler Gamma function and λ is the thermal conductivity

Energy balance

⇓

$$\nabla^2 T(\mathbf{x},t) = \frac{1}{\gamma_\beta} \left({}_C\mathrm{D}_0^{1-\beta} T \right)(\mathbf{x},t)$$

Example of 1D problem

Transient heat 1D problem in cartesian coordinates

$$\frac{\partial^2 T}{\partial x^2} = \frac{1}{\gamma_\beta}\left({}_C\mathrm{D}_0^{1-\beta} T\right)(t) \quad \text{with} \quad 0 \le x < L,\ t > 0,\ 0 \le \beta < 1$$

$$|T|_{x=0} = T_0, \quad \forall t > 0$$

$$|T|_{x=L} = T_0, \quad \forall t > 0$$

$$|T|_{t=0} = F(x) = T_0 + 4(T_0 - T_M)\left[\left(\frac{x}{L}\right)^2 - \frac{x}{L}\right], \quad 0 < x < L$$

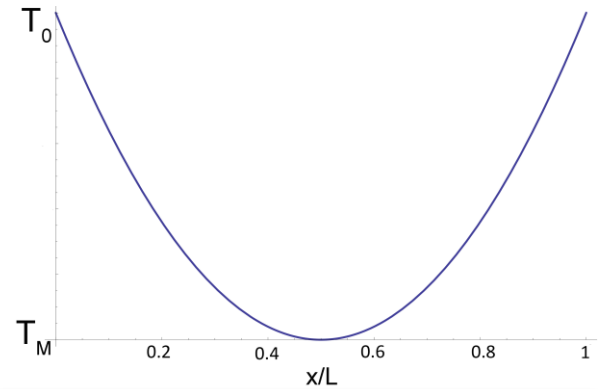

Temperature field at t=0

Solution

$$T(x,t) = T_0 + \sum_{n=1}^{\infty} D_n \sin(\lambda_n x) E_{1-\beta,1}\left[-\lambda_n^2 \gamma_\beta t^{1-\beta}\right]$$

$$E_{\zeta,\eta}(z) = \sum_{n=0}^{\infty} \frac{(z)^n}{\Gamma(\zeta n + \eta)}$$

Example of 1D problem

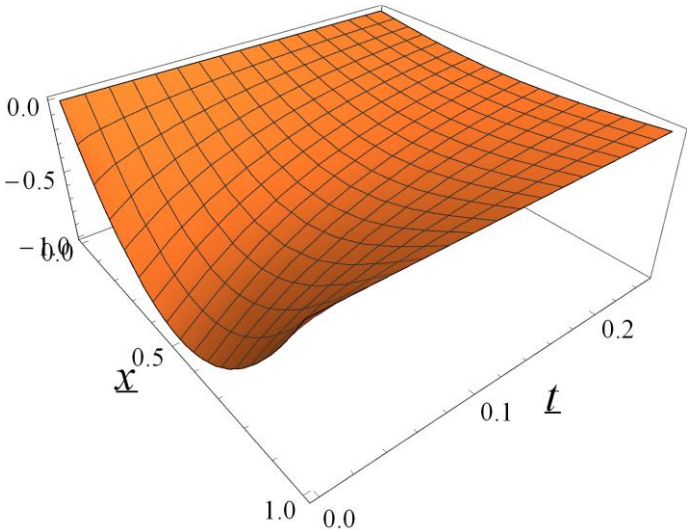

β=0 (Fourier)

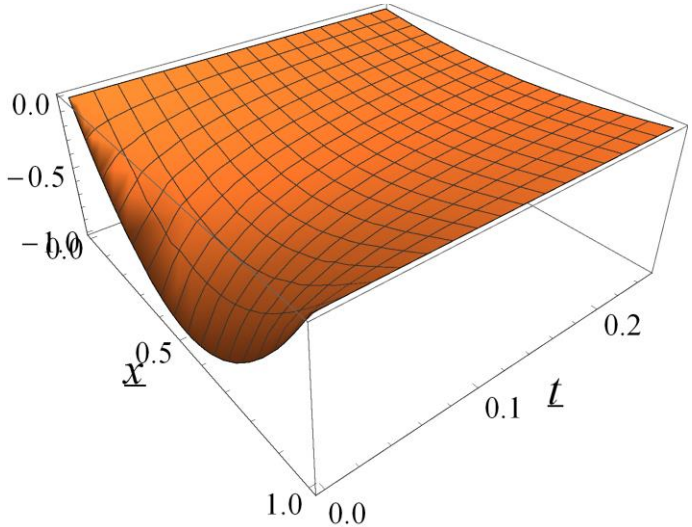

β=0.2

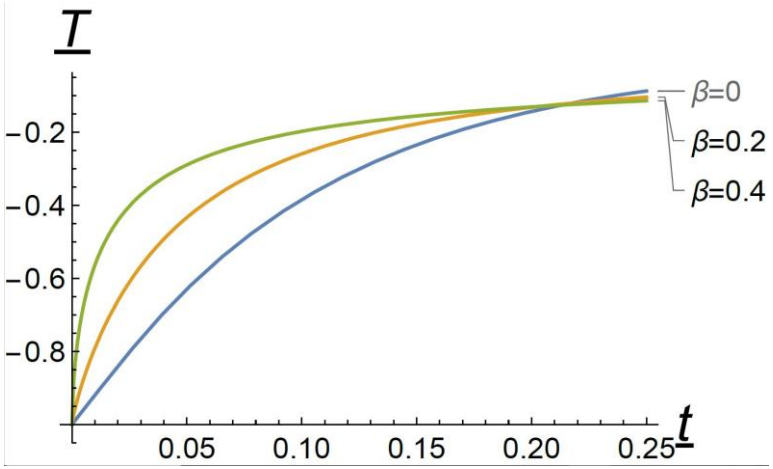

T at x=0.5

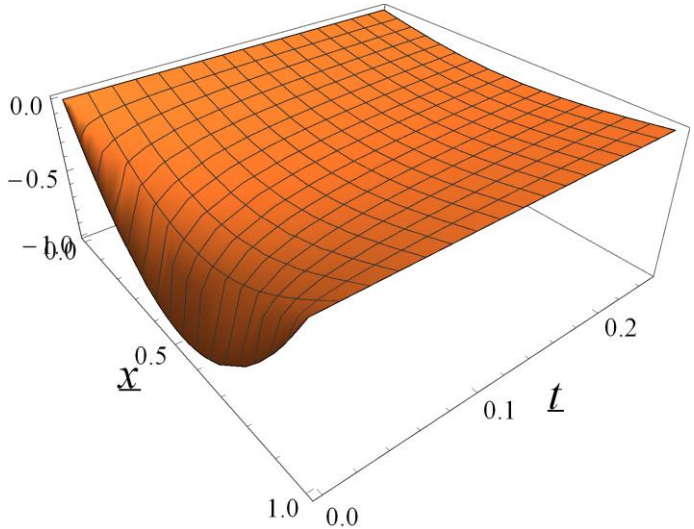

β=0.4

Outline

UNIVERSITÀ DI PAVIA

Medical devices

- Impact of TEVAR on longitudinal strain
- Multi-objective optimization of Nitinol stent design

Non-Fourierian Heat Conduction

- Anomalous heat conduction
- Thermo-mechanical coupling

3D Printing

- Influence of meso-structure and chemical composition on FDM 3D-printed parts

Thermo-mechanical coupling

$$\begin{cases} K_\beta \left({}_C D^\beta_{0+}\right) T_{,xx} - \rho c_v T_{,t} - \alpha E A T_0 u_{,tx} + Q = 0 \\ EA(u_{,xx} - \alpha T_{,x}) + \rho p = 0 \\ N = EA(\varepsilon - \alpha(T - T_0)) \\ \varepsilon = u_{,x} \end{cases}$$

Solution

$$T(x,t) = T_0 + 4(T_0 - T_M) \sum_{m=2}^{\infty} \frac{1}{\pi^2 (m-1)^2} \left(cos\left(\frac{2(m-1)\pi x}{L}\right) - 1 \right) E_{1-\beta,1}\left(-\frac{4(m-1)^2 \pi^2}{L^2 \delta} t^{1-\beta} \right)$$

$$u(x,t) = \alpha (T_0 - T_m) L \sum_{m=2}^{\infty} \frac{1}{\pi^3 (m-1)^3} \sin\left(\frac{2(m-1)\pi x}{L}\right) E_{1-\beta,1}\left(-\frac{4(m-1)^2 \pi^2}{L^2 \delta} t^{1-\beta} \right)$$

$$N(t) = 2 \alpha E A (T_0 - T_M) \sum_{m=2}^{\infty} \frac{1}{\pi^2 (m-1)^2} E_{1-\beta,1}\left(-\frac{4\pi^2 (m-1)^2}{\delta} t^{1-\beta} \right)$$

Results/temperature field

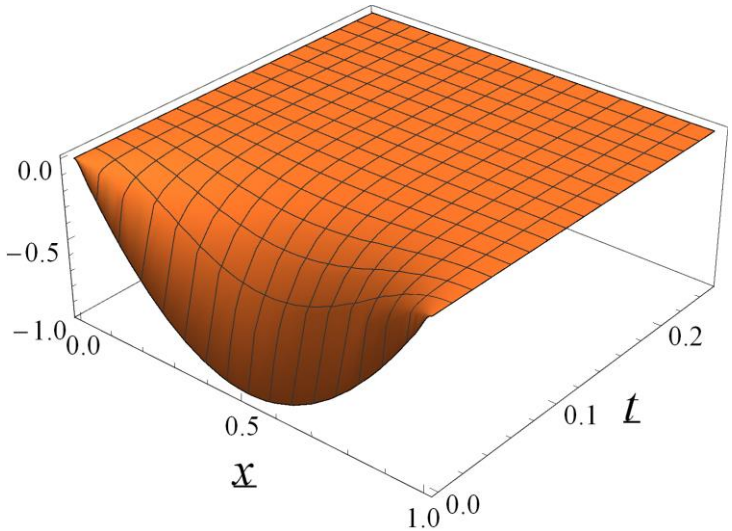

β=0 (Fourier)

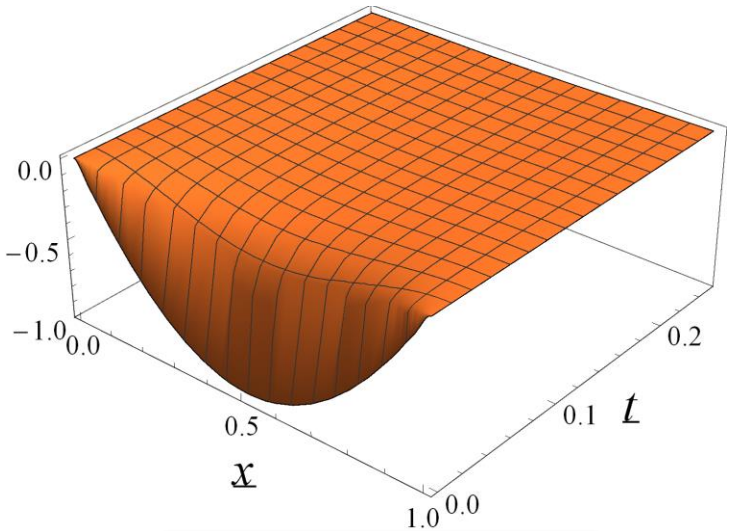

β=0.2

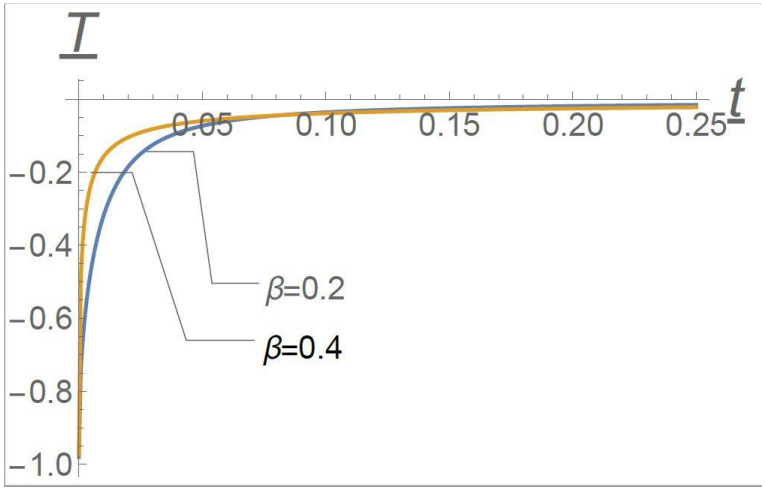

T at x=0.5

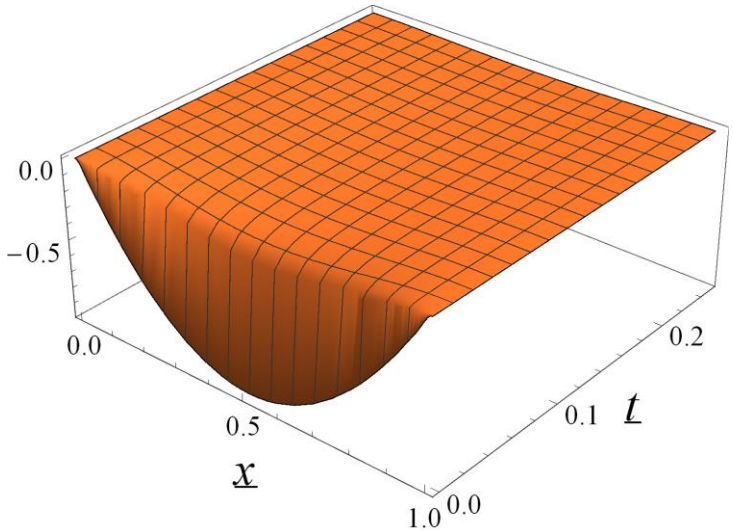

β=0.4

Results/displacement and axial force

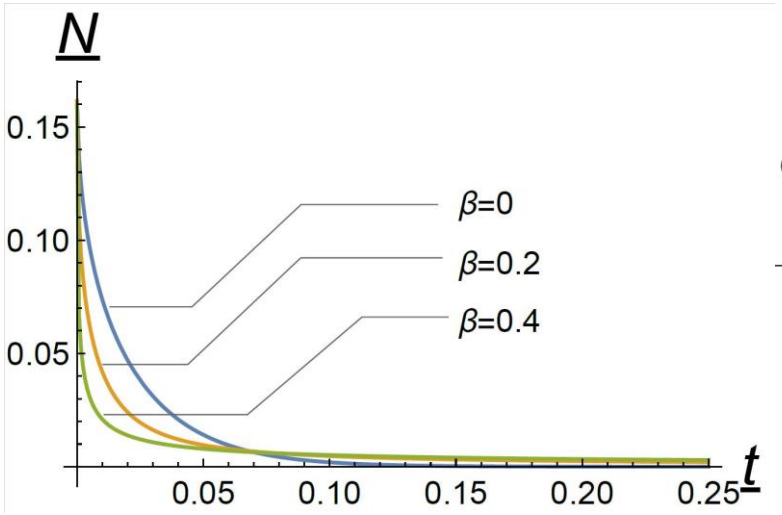

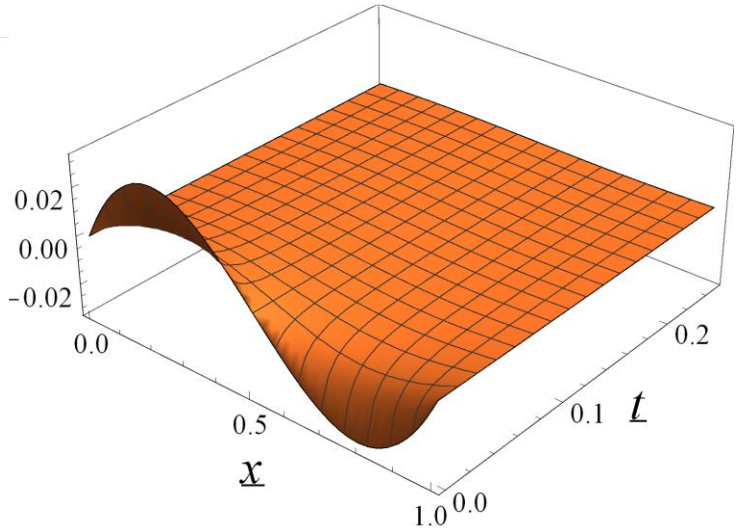

β=0.2

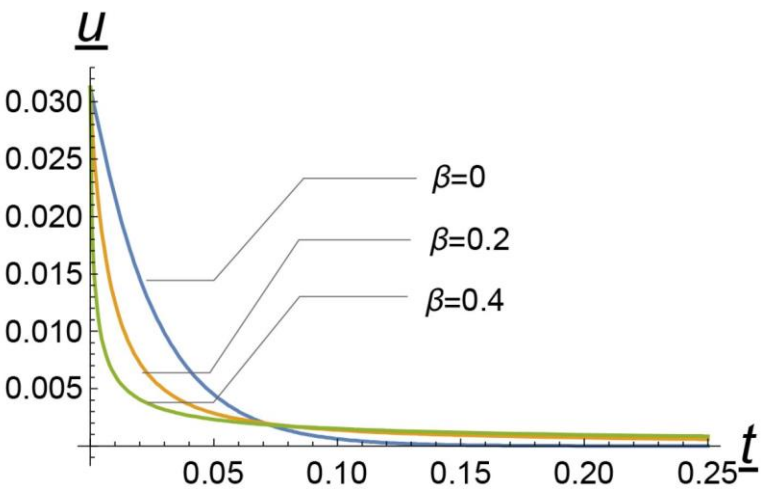

U at x=0.25

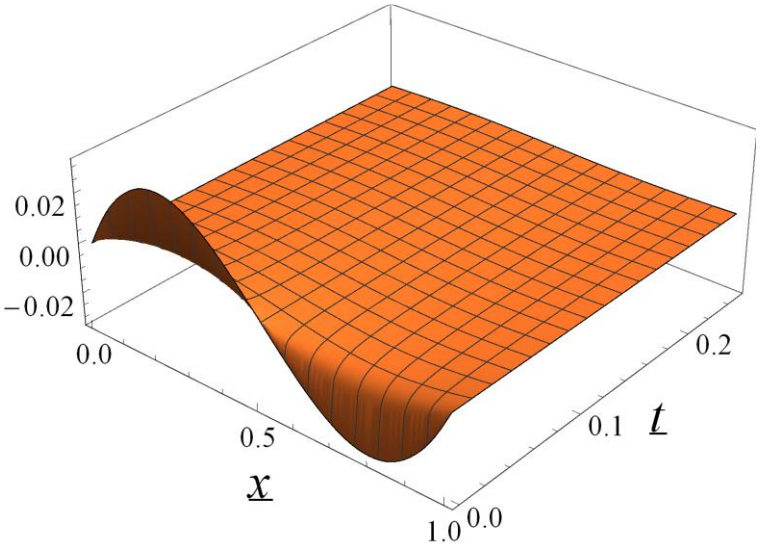

β=0.4

Conclusions

- The solution of the fractional heat equation ($0 < \beta < 1$), governed by Mittag-Leffler functions, exhibits:
  - a *much faster* rising for small times
  - a *much slower* decay for large times

  compared with the solution of classical heat equation

- Thermal steadiness is achieved, by anomalous conductors, employing *longer* times than Fourier ones

- All the resulting fields, namely the axial stress, the displacement, and the temperature, are influenced by the thermal and elastic deformability of the bar. The higher is the deviation from the Fourier-like behavior, the more rapid becomes the rise in time

Outline

UNIVERSITÀ DI PAVIA

Medical devices

- Impact of TEVAR on longitudinal strain
- Multi-objective optimization of Nitinol stent design

Non-Fourierian Heat Conduction

- Anomalous heat conduction
- Thermo-mechanical coupling

3D Printing

- Influence of meso-structure and chemical composition on FDM 3D-printed parts

Advantages of 3D-printing:

- Complex geometry
- Accurate printing
- Less waste material
- Short time-to-market
- Many available materials, included biocompatible ones

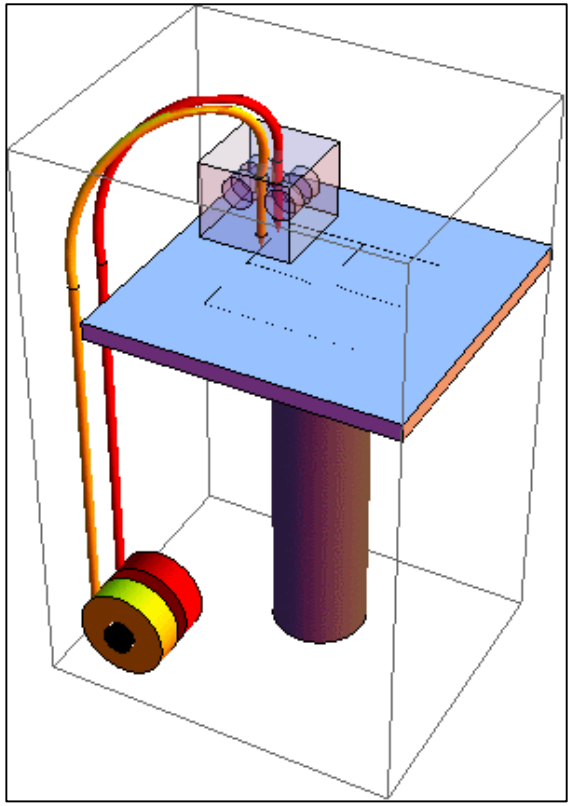

Fused Deposition Modeling (FDM)

Thermoplastic filament

↓

Heated extruder

↓

Deposition of semi-molten material on the build surface

↓

Movement in X and Y directions

↓

Build surface lowered in Z direction

↓

Resulting 3d-printed FDM object

FDM parts meso-structure

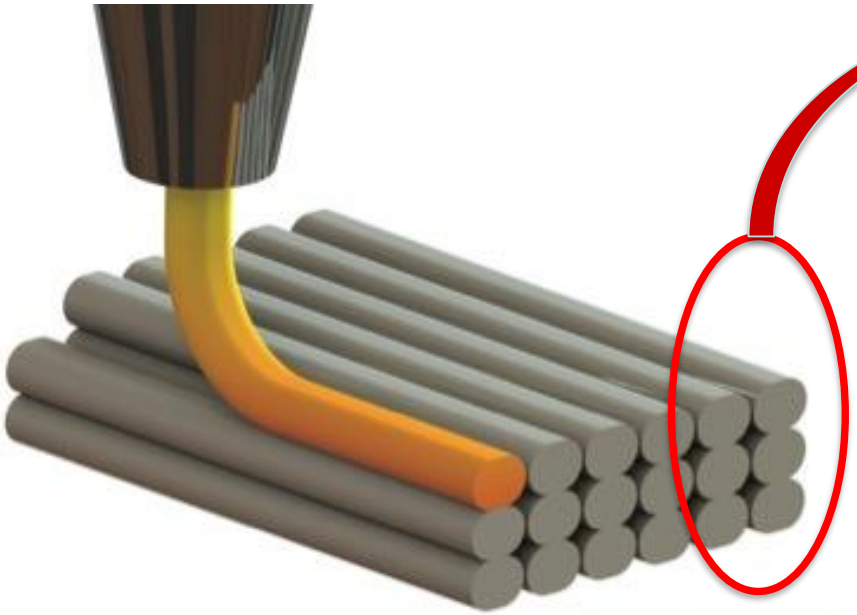

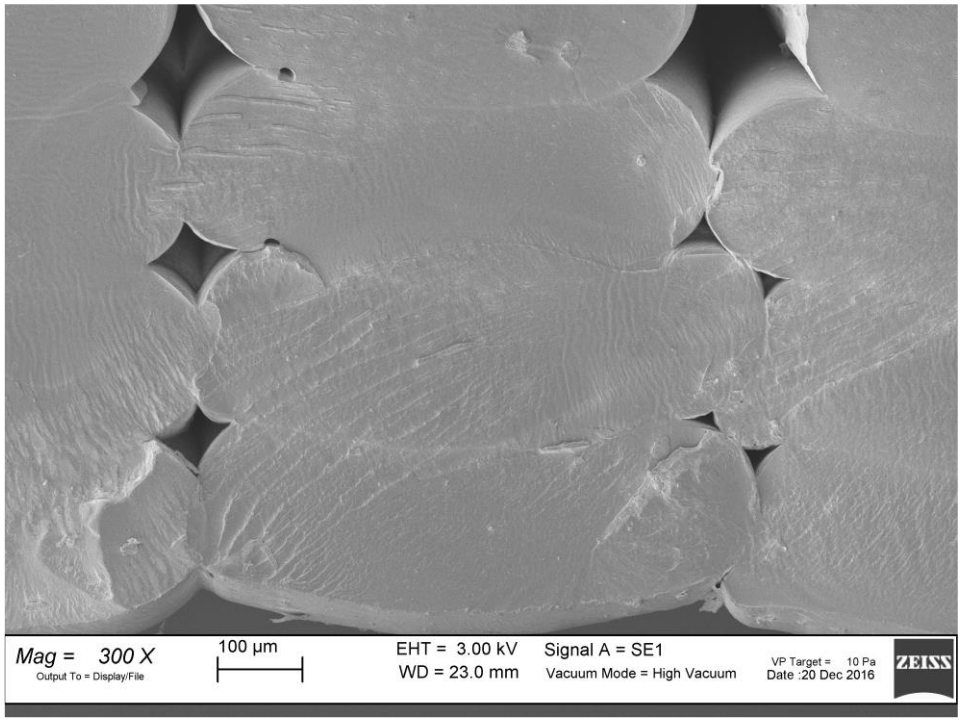

Goal: Investigate how filament dimensions , orientation and chemical composition affect the FDM 3D-printed part mechanical properties

Inner structure at a sub-millimeter scale resulting from FDM extrusion process

ABS properties investigated:

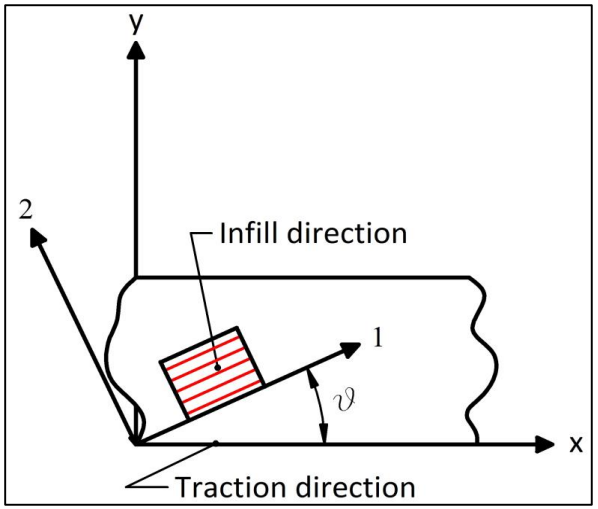

Mechanical behaviour evaluation	**Material strength** evaluation
Classical Lamination Theory (CLT)	**Tsai-Hill failure criterion**
Four elastic constants required: ➢ E_1: longitudinal Young's modulus ➢ E_2: transverse Young's modulus ➢ ν_{12}: major Poisson's ratio ➢ G_{12}: shear modulus	Three admissible stresses required: ➢ S_1: strength in the fiber direction ($\theta=0°$) ➢ S_2: strength in the transverse direction ($\theta=90°$) ➢ S_{12}: in-plane shear strength ($\theta=45°$)

Methods

Specimen **features**:

- **Unidirectional fibers**
- **Fibers aligned** in the plane
- **10% overlap** between fibers
- **No perimeters**

Five different **fiber orientations (*θ*)** have been considered:

- 0°
- 45°
- 90°

} **mechanical properties**

- 20°
- 70°

} **validate experimental data**

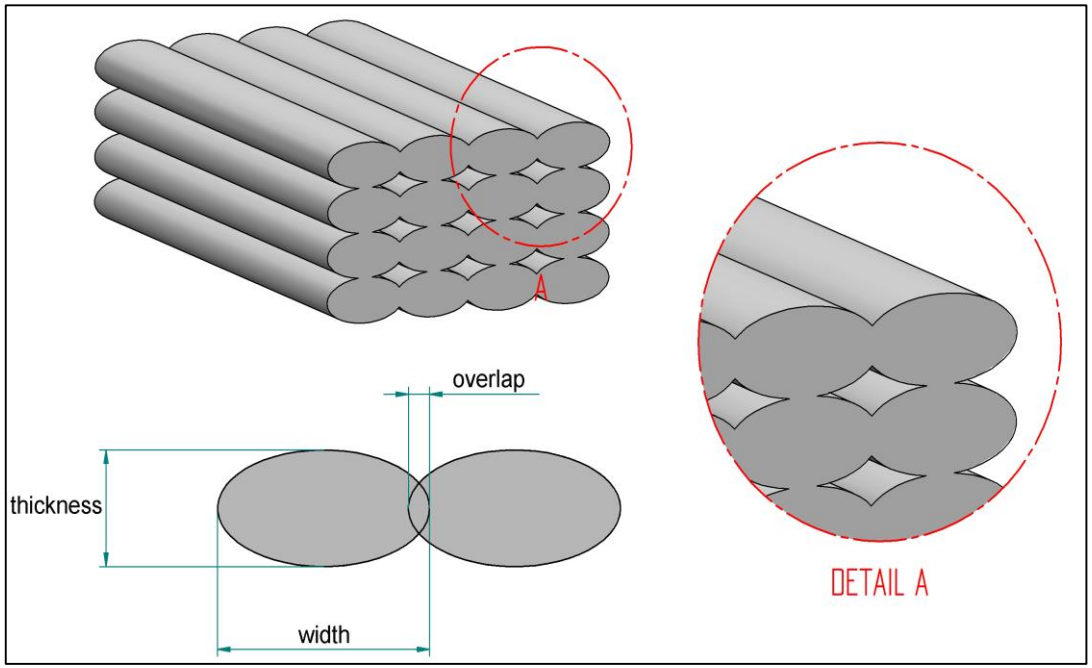

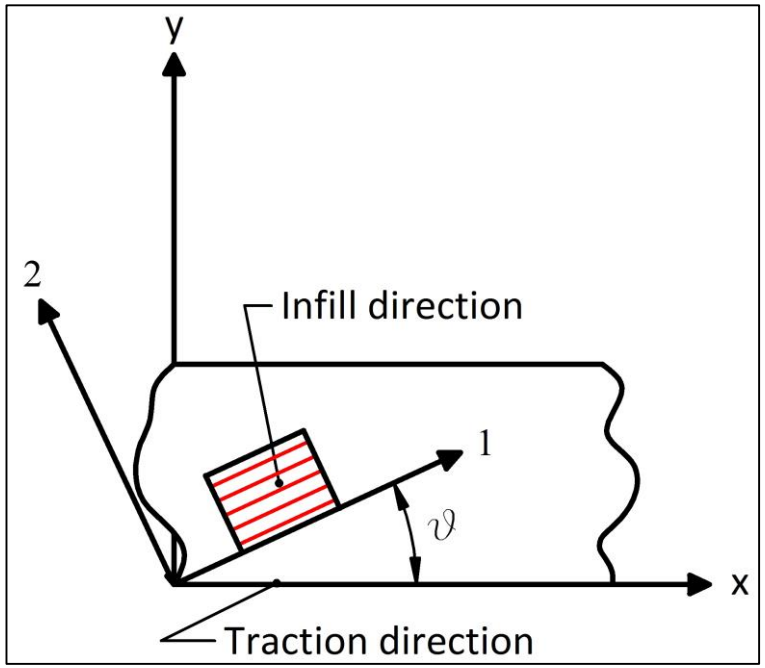

Tensile test

Two different types of ABS have been tested, in **different configurations**:

Configurations	Type	Layer Height (mm)	Extrusion Width (mm)
A1	B432	0,2	0,4
A2	B432	0,25	0,5
A3	B432	0,3	0,6
B1	B322	0,2	0,4

Tensile test features:

- Displacement control
- Test running time: 1-10 min
- Displacement rate: 2 mm/min
- Gage length: 30-50 mm

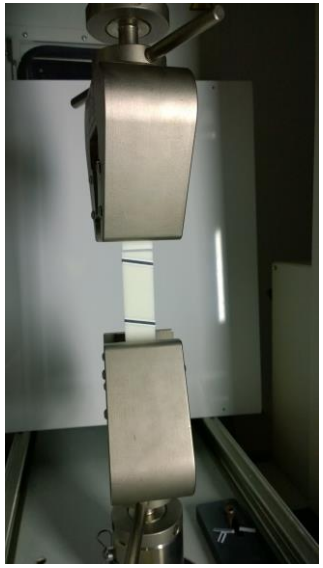

Results – Elastic modulus

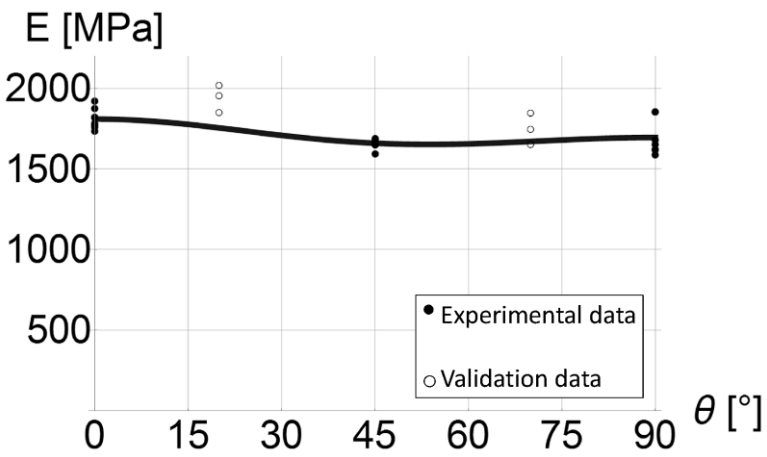

A1 – B432 – 0.2 x 0.4 mm

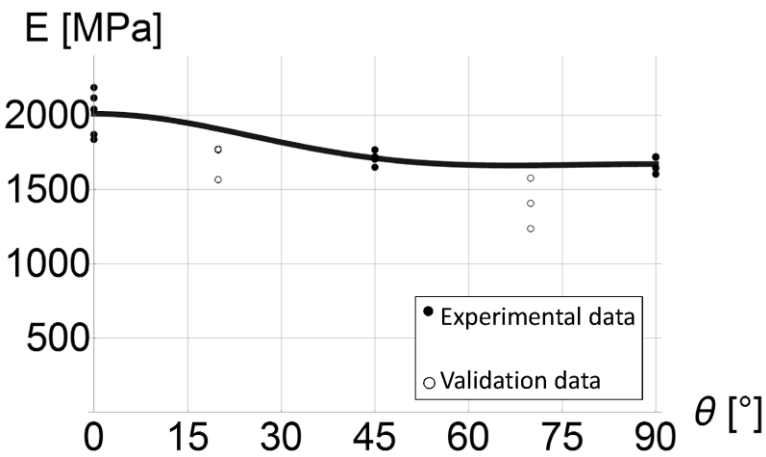

A2 – B432 – 0.25 x 0.5 mm

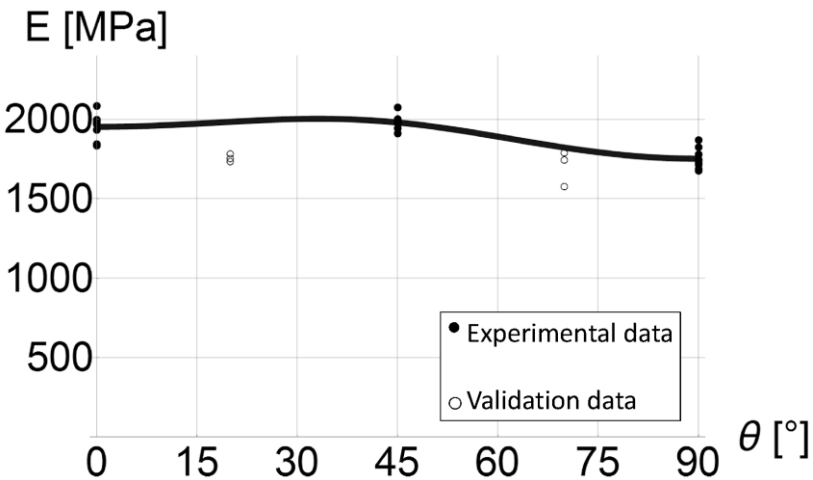

A3 – B432 – 0.3 x 0.6 mm

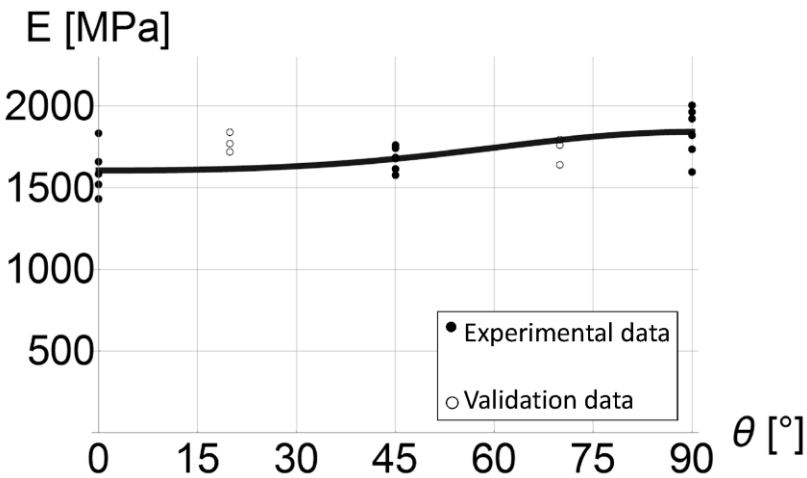

B1 – B322 – 0.2 x 0.4 mm

Results – Yield stress

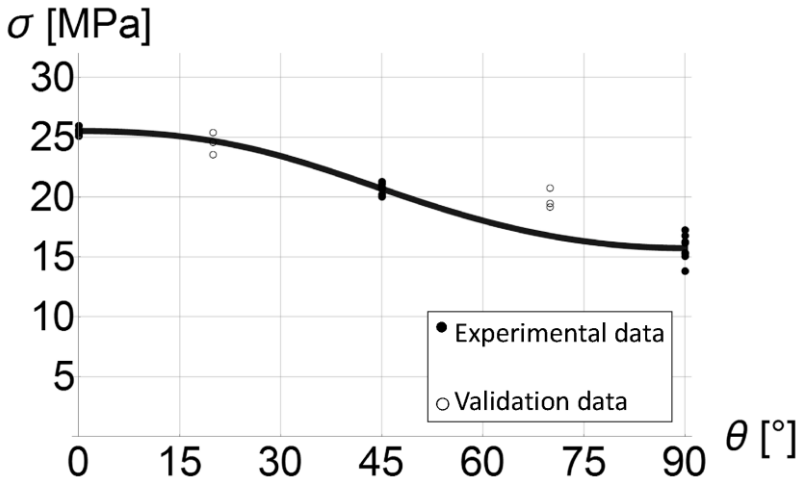

A1 – B432 – 0.2 x 0.4 mm

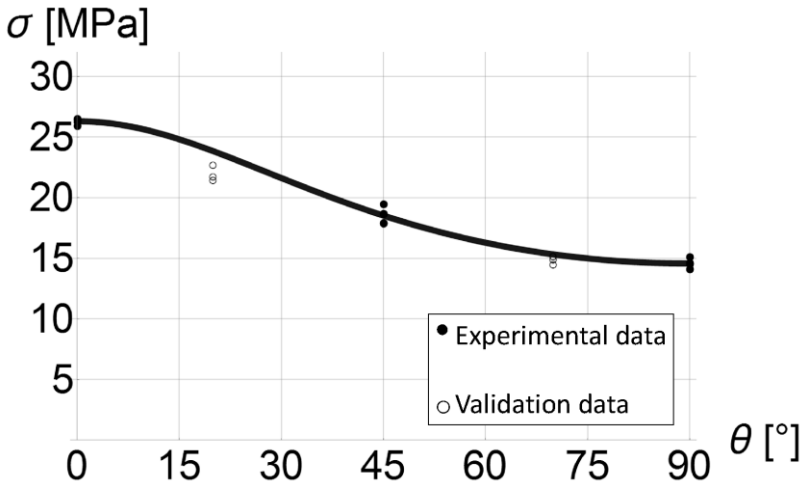

A2 – B432 – 0.25 x 0.5 mm

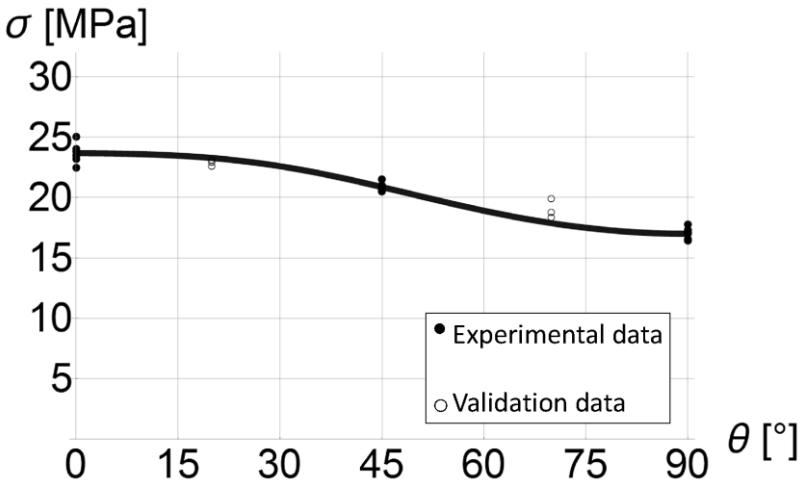

A3 – B432 – 0.2 x 0.4 mm

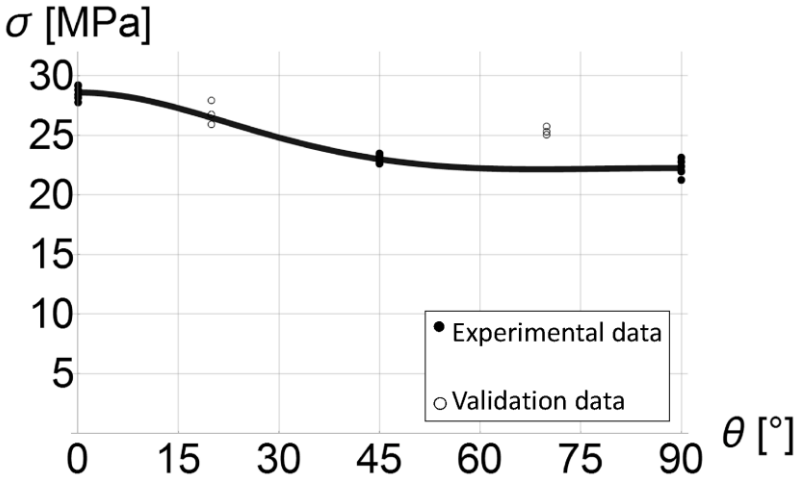

B1 – B322 – 0.2 x 0.4 mm

Conclusions

- We investigated how fiber orientation, filament dimensions and chemical composition affect the mechanical properties of ABS 3D-printed components

- We verified that a 3D-printed FDM material shows anisotropic mechanical properties

- CLT and Tsai-Hill yielding theory were found to be well capable of predicting in-plane stiffness and strength at the macro-scale

Thanks for your attention

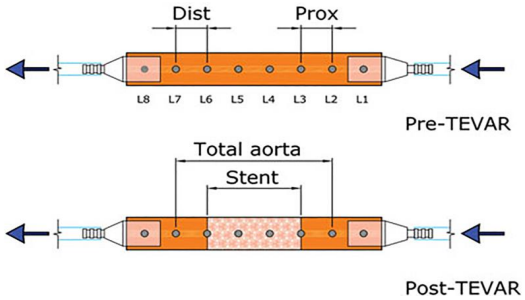

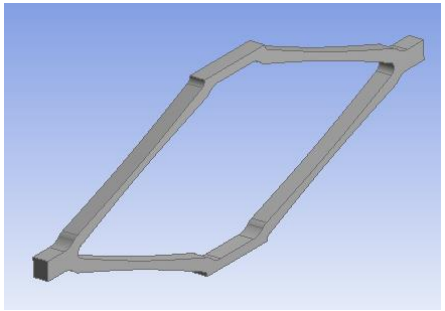

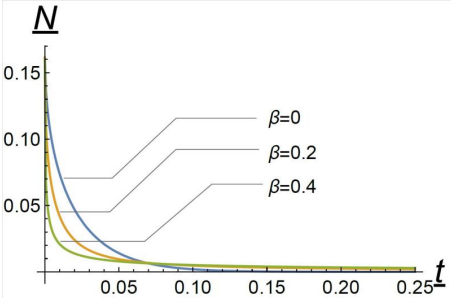

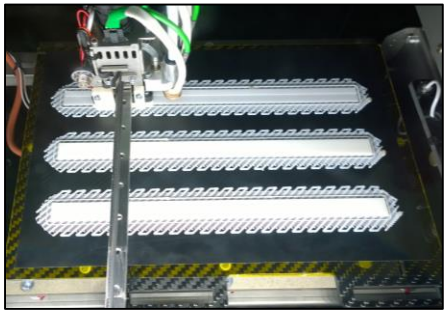

Results – Yield stress

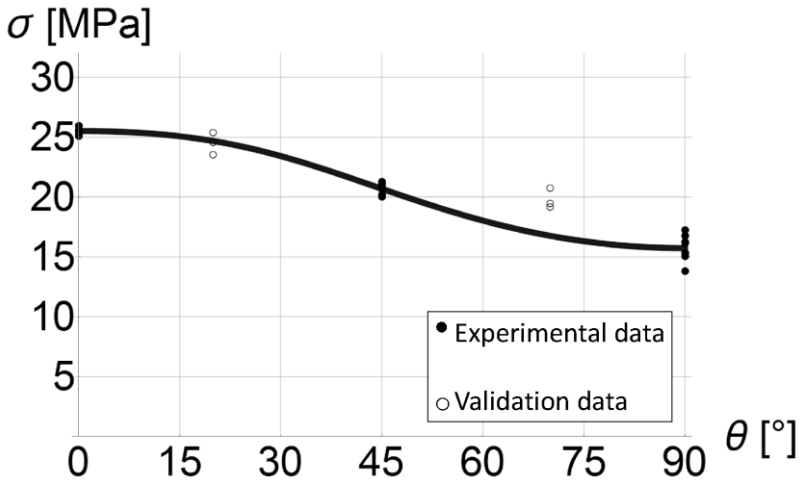

A1 – B432 – 0.2 x 0.4 mm

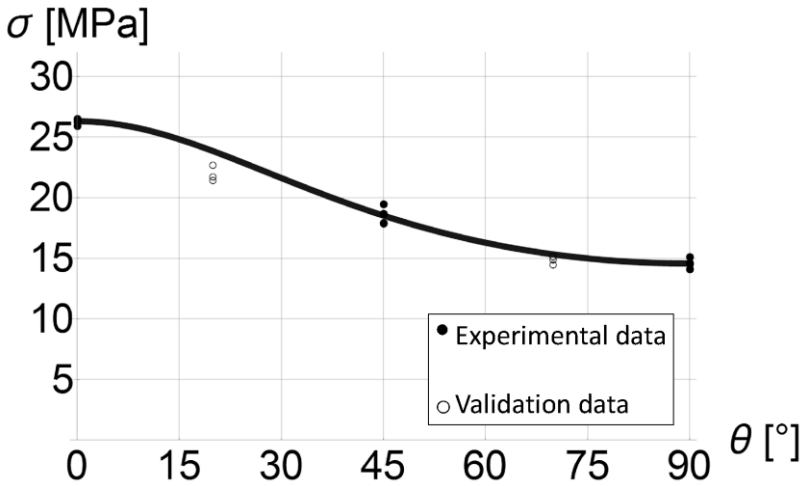

A2 – B432 – 0.25 x 0.5 mm

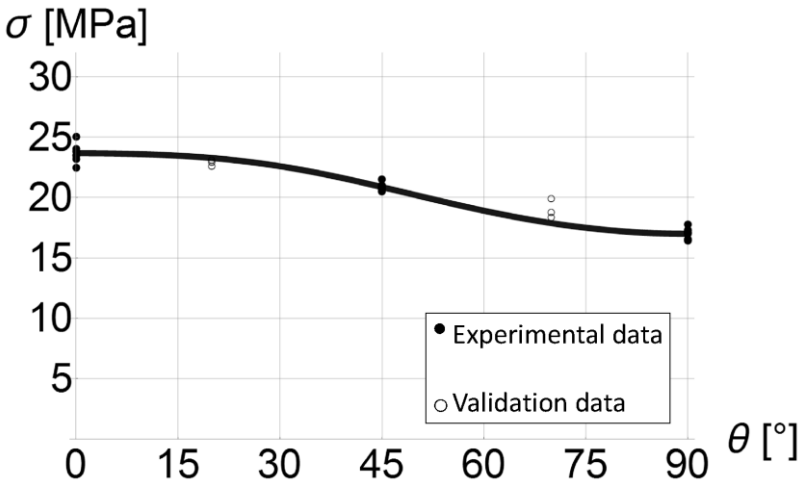

A3 – B432 – 0.2 x 0.4 mm

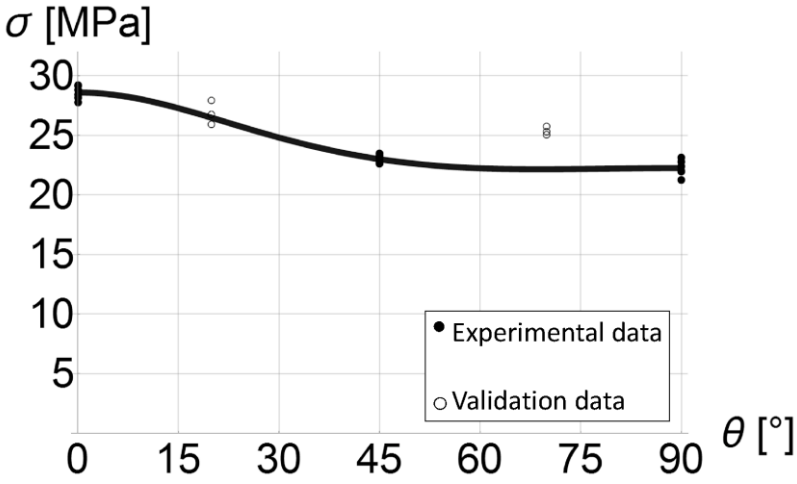

B1 – B322 – 0.2 x 0.4 mm

Enhanced Design

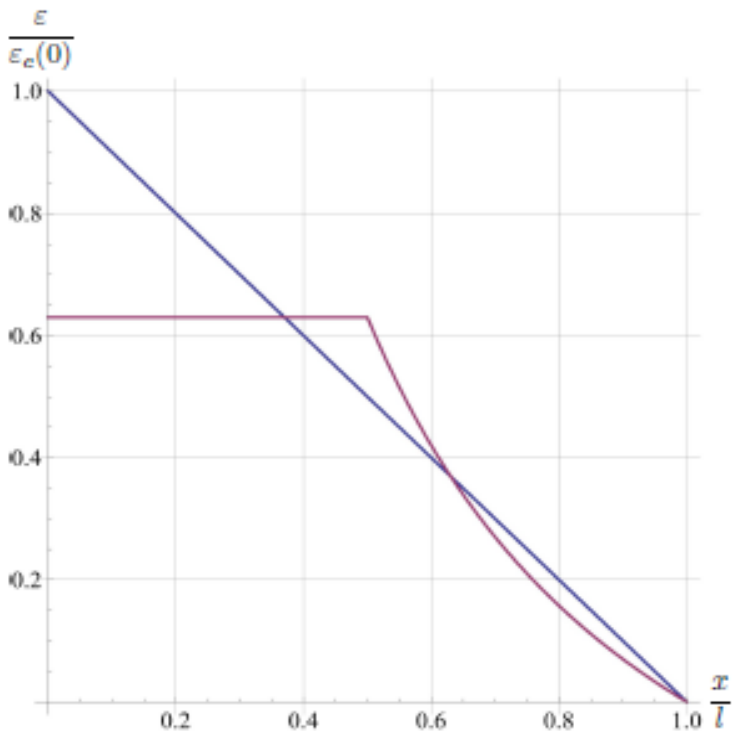

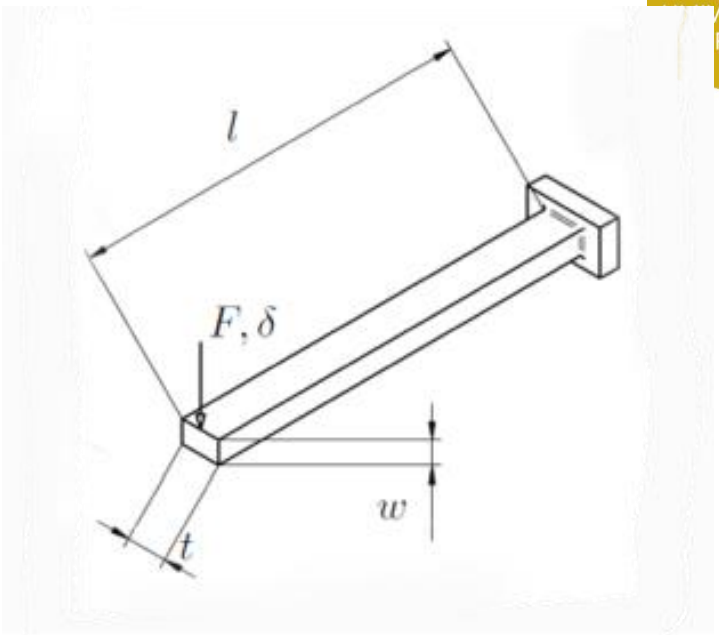

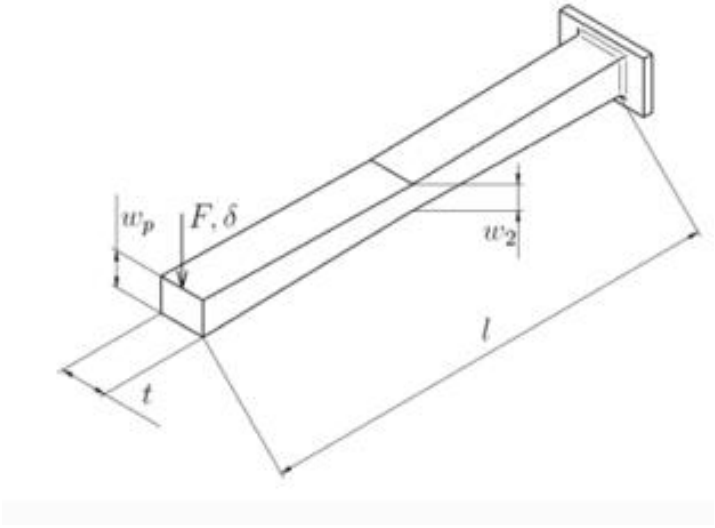

Examples of «anomalous» heat transfer

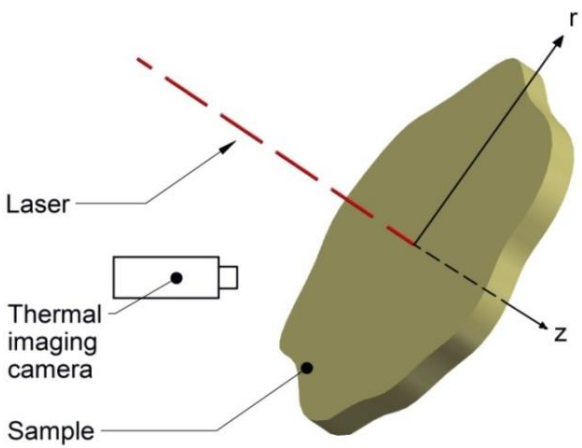

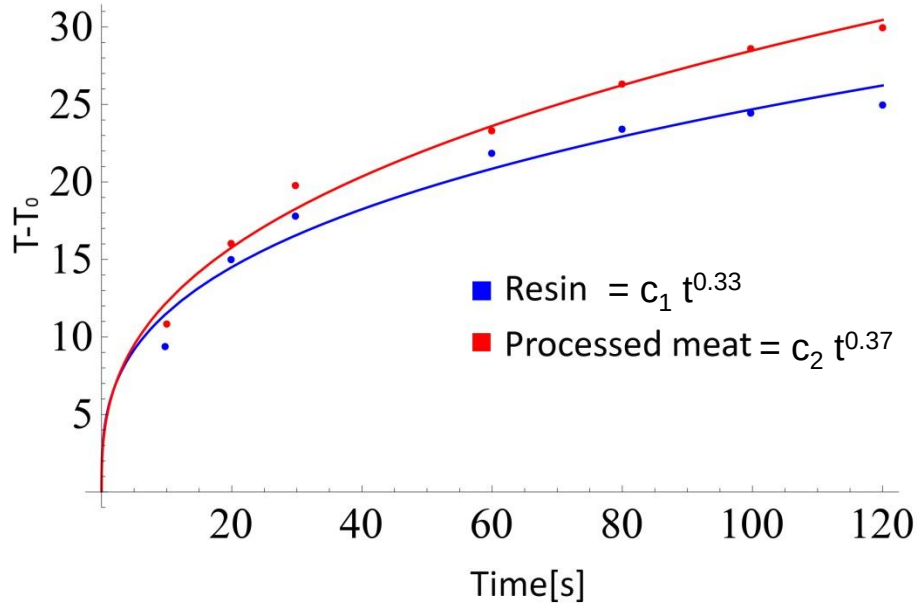

[Banerjee et al. , 2008]

The temperature evolution for an unit step LPR power source follows a power law of time <u>different than expected by the Fourier law that is exponential</u>

Therefore, the temperature evolution due to a generic LPR power history is a convolution integral with power law kernel. FRACTIONAL DERIVATIVE?

Constitutive law for FDM parts

We use CLT and Tsai-Hill yielding criterion in finite element analysis to predict FDM parts mechanical behavior. Both models are calibrated using experimental data

Linear elastic mechanical behaviour

↓

Classical Lamination Theory (CLT)

↓

Four elastic constants required:

- E_1 = elastic tensile modulus in material direction 1
- E_2 = elastic tensile modulus in material direction 2
- ν_{12} = ratio between strain in direction 2 and strain in direction 1
- G_{12} = shear modulus in plane 12

Plastic mechanical behaviour

↓

Tsai-Hill yielding surface

↓

Three admissible stresses required:

- σ_1 = maximum tensile stress in material direction 1
- σ_2 = maximum tensile stress in material direction 2
- τ_{12} = maximum shear stress value in plane 12

UNIVERSITÀ DI PAVIA

Classical Lamination Theory (CLT)

$\theta=0°$	→	E_1 , ν_{12}
$\theta=90°$	→	E_2
$\theta=45°$	→	G_{12}

Orthotropic fiber (layer) under plane stress

$$\begin{bmatrix}\sigma_1\\ \sigma_2\\ \tau_{12}\end{bmatrix} = \frac{1}{1-\nu_{12}\nu_{21}}\begin{bmatrix}E_1 & \nu_{12}E_2 & 0\\ \nu_{12}E_2 & E_2 & 0\\ 0 & 0 & G_{12}(1-\nu_{12}\nu_{21})\end{bmatrix}\begin{bmatrix}\varepsilon_1\\ \varepsilon_2\\ \gamma_{12}\end{bmatrix}$$

Elastic moduli for ABS 3D-printed specimen through Classical Lamination Theory

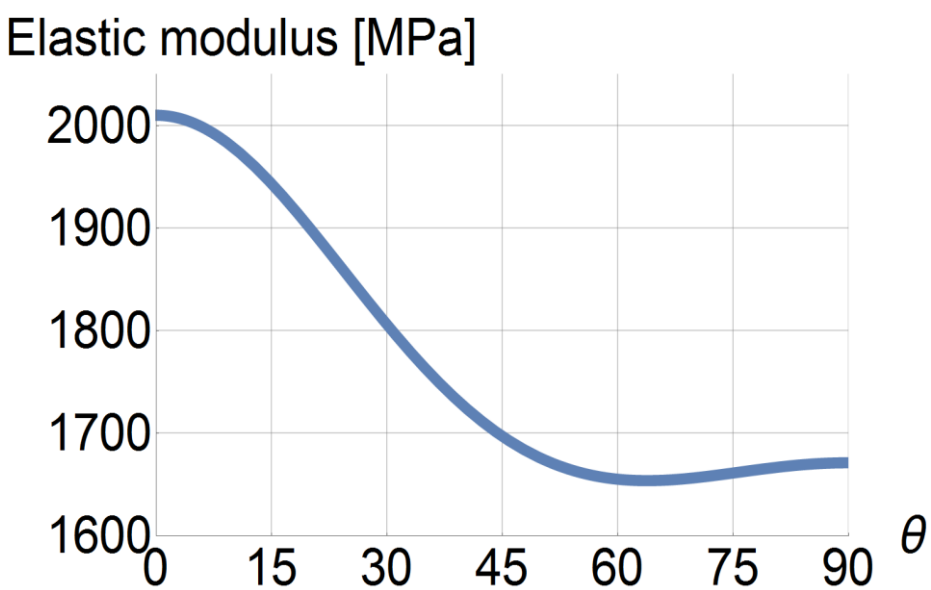

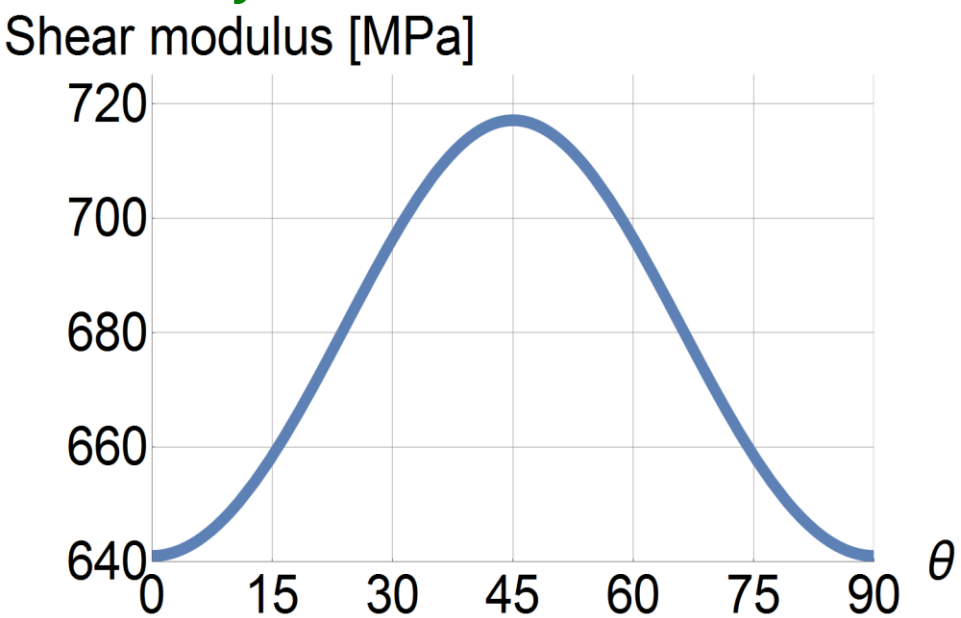

Yielding criterion for FDM parts

Formulation of suitable yielding criteria, using Tsai-Hill approach

$\theta=0°$	→	s_{Lt}
$\theta=90°$	→	s_{Tt}
$\theta=45°$	→	s_{LTs}

Tsai-Hill criterion: failure occurs in an orthotropic lamina when

$$\frac{\sigma_1^2}{S_{Lt}^2} - \frac{\sigma_1\sigma_2}{S_{Lt}^2} + \frac{\sigma_2^2}{S_{Tt}^2} + \frac{\tau_{12}^2}{S_{LTs}^2} = 1$$

Uniaxial tensile strength according to Tsai – Hill Theory

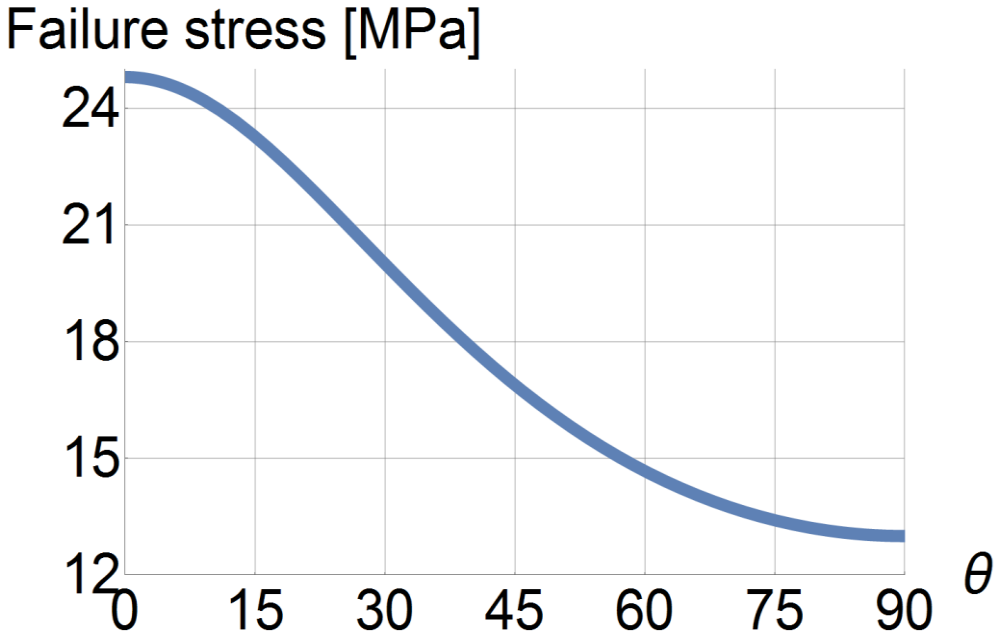

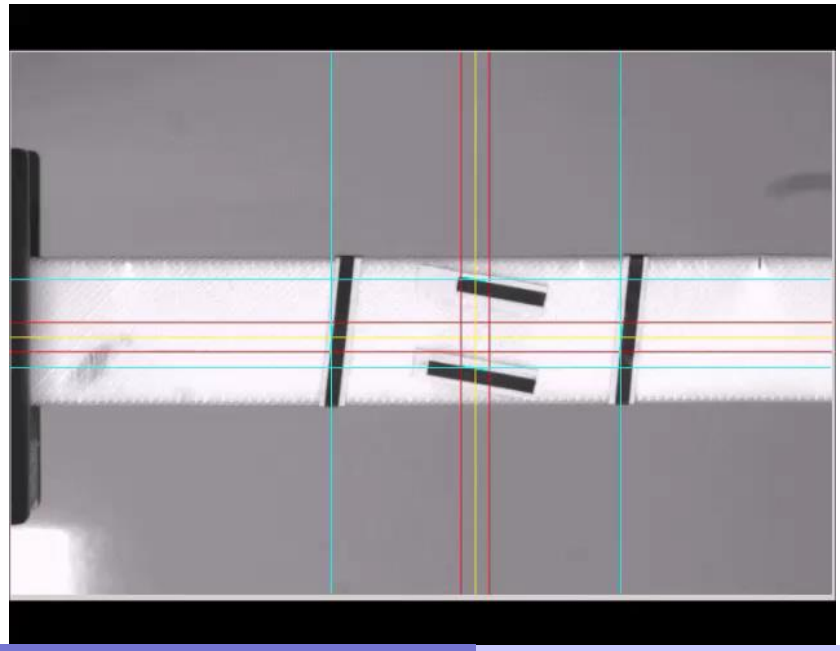

Validation: experimental data vs FEA

Plate with hole - two cases considered:

Circular hole

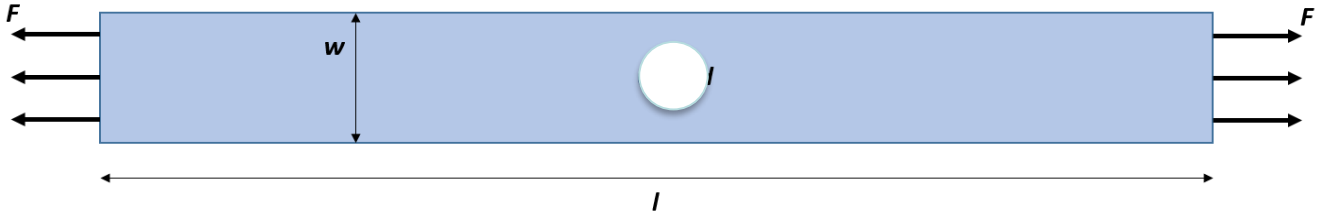

Elliptic hole

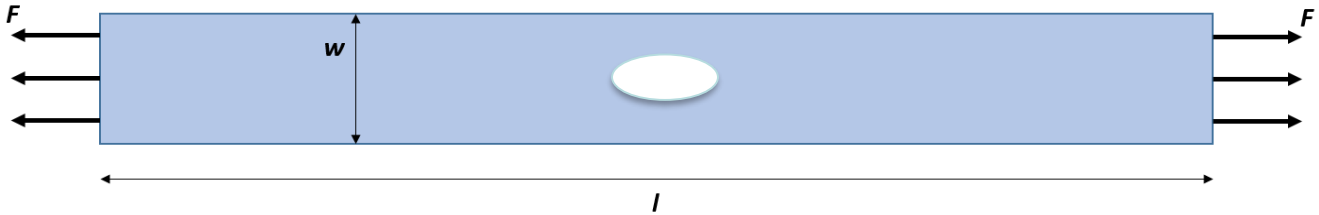

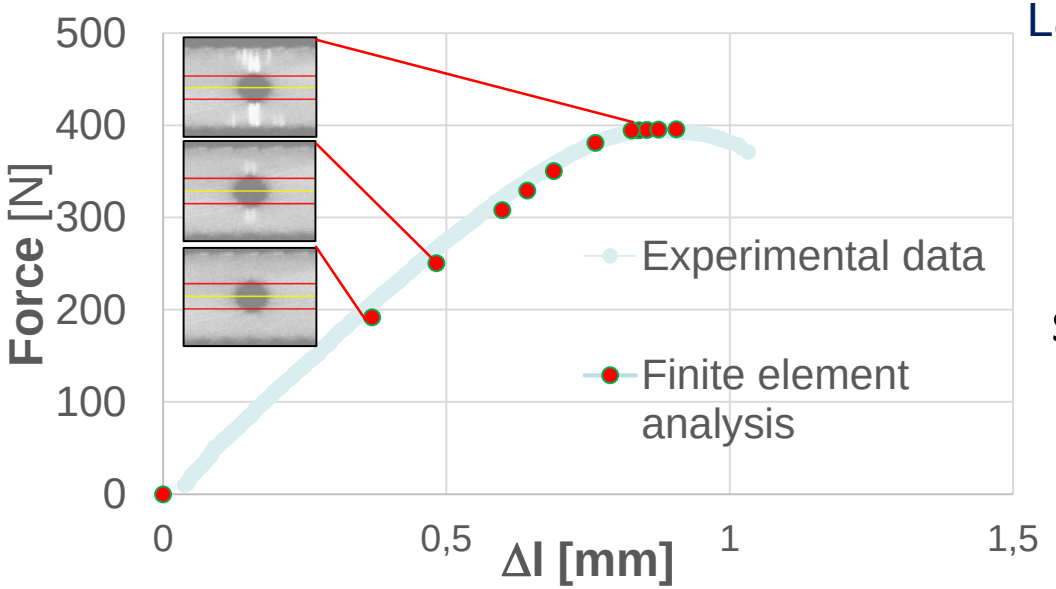

Layer sequence through the thickness

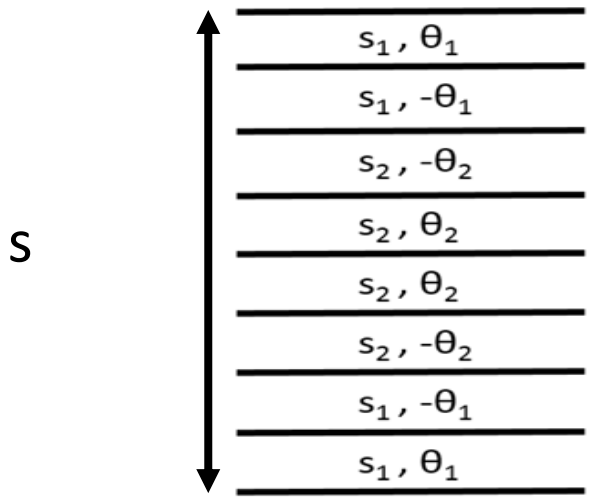

Ansys commercial software – two type of elements considered

Solid 186: 3D 20-node layered element that exhibits quadratic displacement behavior

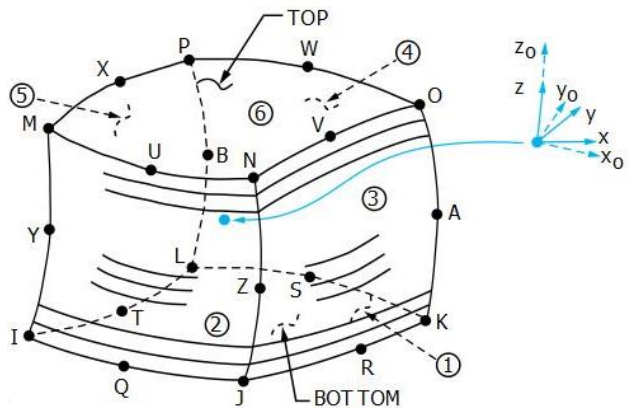

Shell 181: 4-node layered element with six DOF at each node

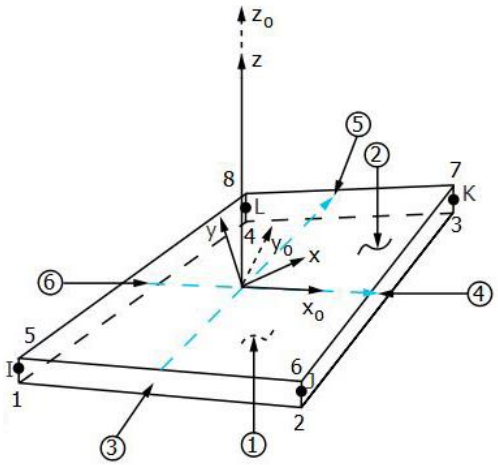

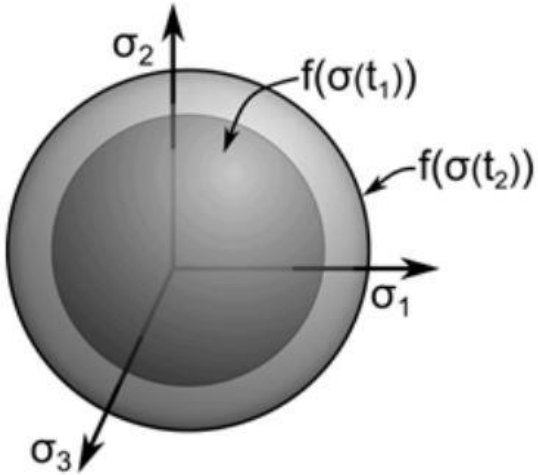

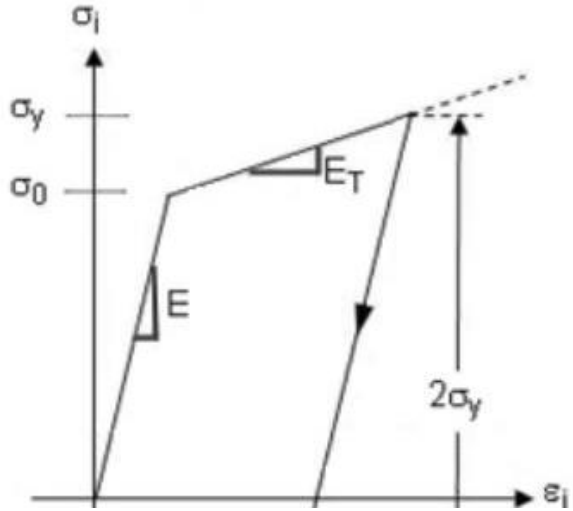

- **Large displacements**
- **Plasticity with isotropic hardening rule**

Load [N] – displacement [mm] curve

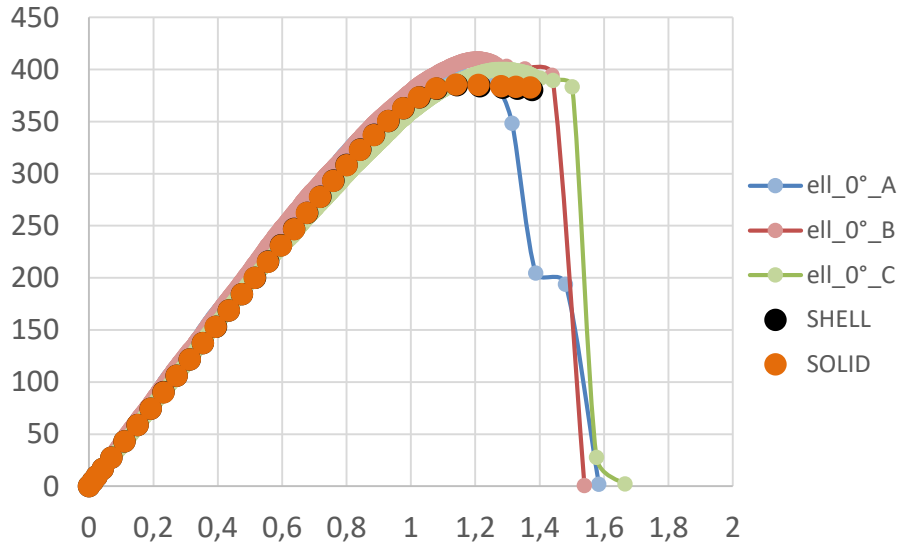

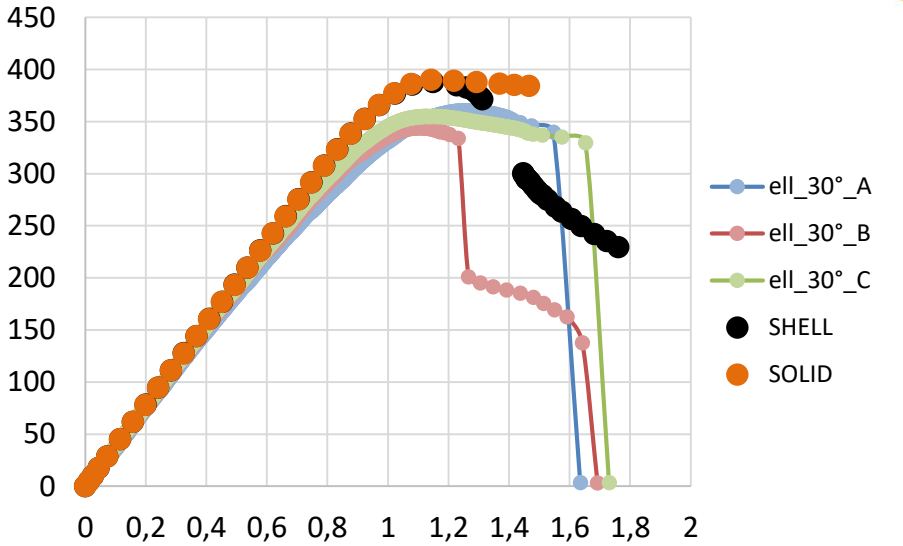

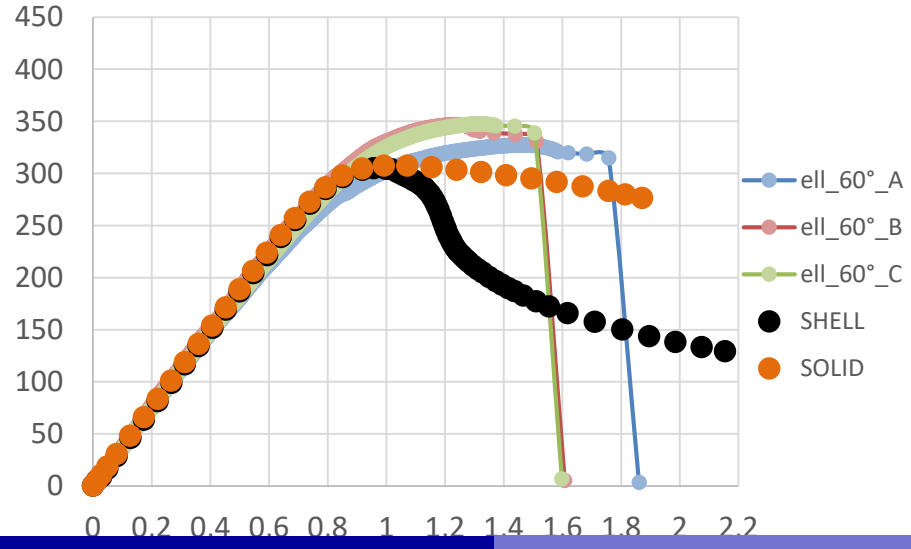

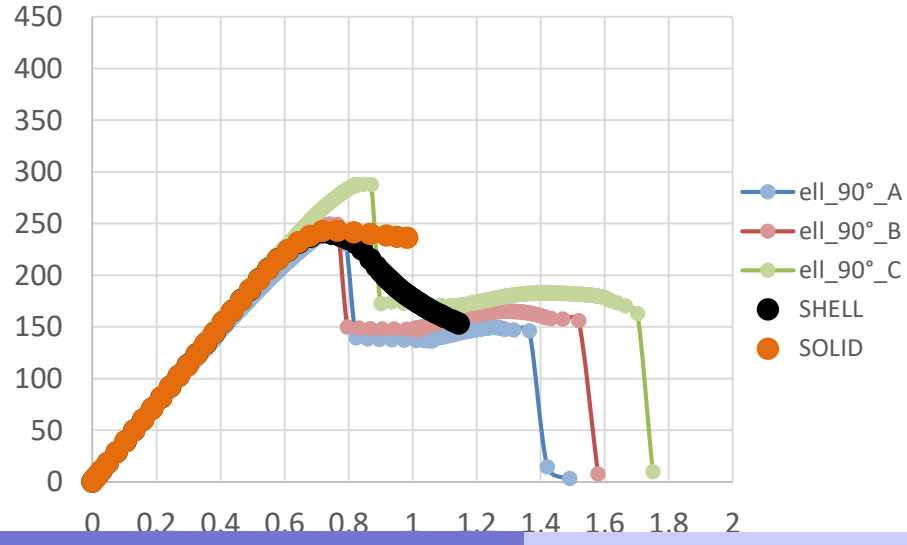

Validation - Plate with elliptical hole

Using 8 elements through the tickness (1 element for each layer) the response curve is almost the same

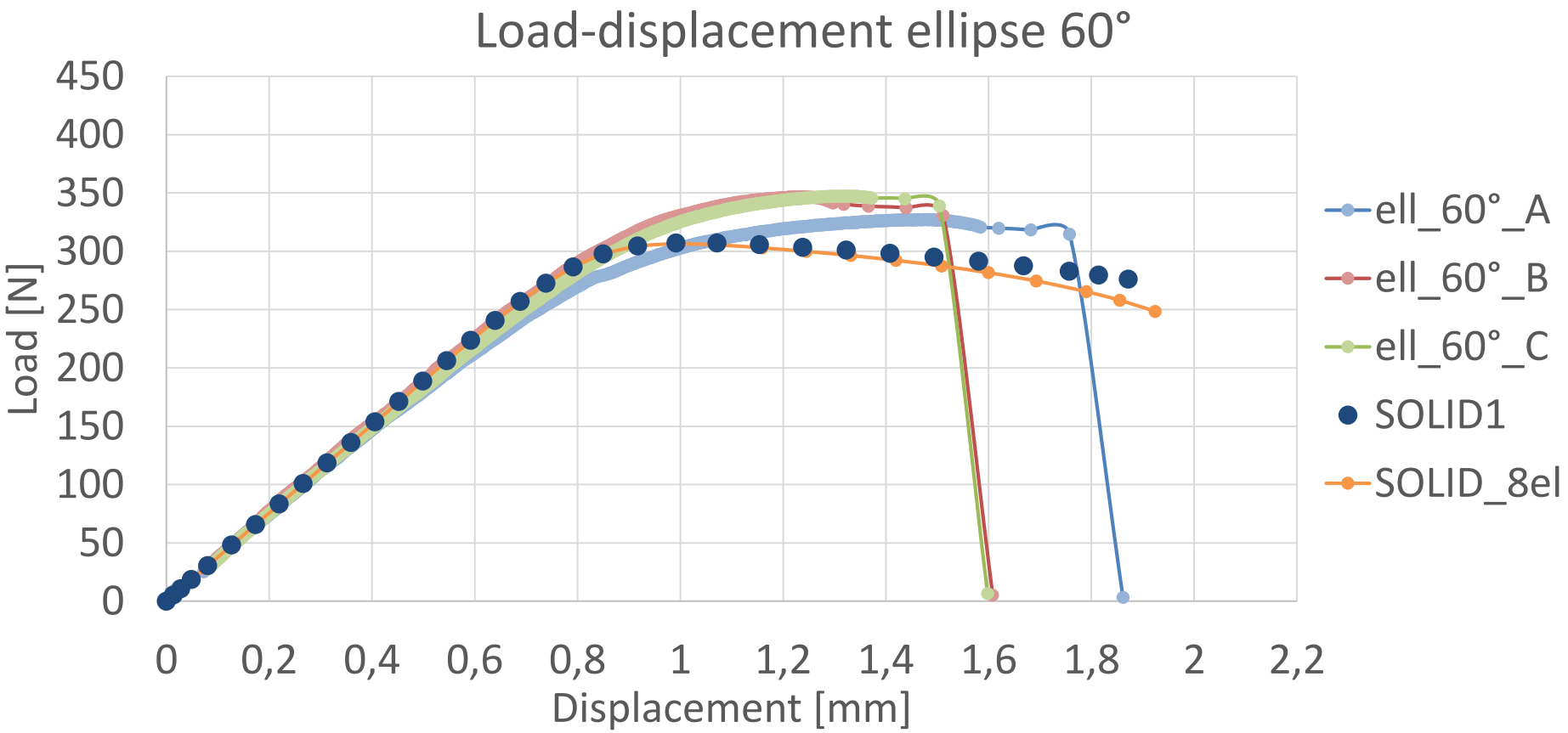

UNIVERSITÀ DI PAVIA

Conclusions:

- **CLT has seems to be accurate enough in predicting mechanical response in elastic domain using both shell and solid elements.**
- **In plastic region the simulated response curve does not accurately match experimental data. Solid elements are more precise.**
- **More accurate or different constitutive models are needed to capture mechanical response in plastic region**